Nutrient-sensing growth hormone secretagogue receptor in macrophage programming and meta-inflammation

Da Mi Kim [1,9], Jong Han Lee [2,3,9], Quan Pan [1], Hye Won Han [1], Zheng Shen [1], Sahar Eshghjoo [4,5], Chia-Shan Wu [1,3], Wanbao Yang [1], Ji Yeon Noh [1], David W. Threadgill [1,6], Shaodong Guo [1], Gus Wright [7], Robert Alaniz [4,8], Yuxiang Sun [1,3,]*

ABSTRACT

Objective: Obesity-associated chronic inflammation, aka meta-inflammation, is a key pathogenic driver for obesity-associated comorbidity. Growth hormone secretagogue receptor (GHSR) is known to mediate the effects of nutrient-sensing hormone ghrelin in food intake and fat deposition. We previously reported that global *Ghsr* ablation protects against diet-induced inflammation and insulin resistance, but the site(s) of action and mechanism are unknown. Macrophages are key drivers of meta-inflammation. To unravel the role of GHSR in macrophages, we generated myeloid-specific *Ghsr* knockout mice (*LysM-Cre;Ghsr^f/f^*).

Methods: *LysM-Cre;Ghsr^f/f^* and control *Ghsr^f/f^* mice were subjected to 5 months of high-fat diet (HFD) feeding to induce obesity. *In vivo*, metabolic profiling of food intake, physical activity, and energy expenditure, as well as glucose and insulin tolerance tests (GTT and ITT) were performed. At termination, peritoneal macrophages (PMs), epididymal white adipose tissue (eWAT), and liver were analyzed by flow cytometry and histology. For *ex vivo* studies, bone marrow-derived macrophages (BMDMs) were generated from the mice and treated with palmitic acid (PA) or lipopolysaccharide (LPS). For *in vitro* studies, macrophage RAW264.7 cells with *Ghsr* overexpression or Insulin receptor substrate 2 (*Irs2*) knockdown were studied.

Results: We found that *Ghsr* expression in PMs was increased under HFD feeding. *In vivo*, HFD-fed *LysM-Cre;Ghsr^f/f^* mice exhibited significantly attenuated systemic inflammation and insulin resistance without affecting food intake or body weight. Tissue analysis showed that HFD-fed *LysM-Cre;Ghsr^f/f^* mice have significantly decreased monocyte/macrophage infiltration, pro-inflammatory activation, and lipid accumulation, showing elevated lipid-associated macrophages (LAMs) in eWAT and liver. *Ex vivo*, *Ghsr*-deficient macrophages protected against PA- or LPS-induced pro-inflammatory polarization, showing reduced glycolysis, increased fatty acid oxidation, and decreased NF-κB nuclear translocation. At molecular level, GHSR metabolically programs macrophage polarization through PKA-CREB-IRS2-AKT2 signaling pathway.

Conclusions: These novel results demonstrate that macrophage GHSR plays a key role in the pathogenesis of meta-inflammation, and macrophage GHSR promotes macrophage infiltration and induces pro-inflammatory polarization. These exciting findings suggest that GHSR may serve as a novel immunotherapeutic target for the treatment of obesity and its associated comorbidity.

© 2023 The Authors. Published by Elsevier GmbH. This is an open access article under the CC BY-NC-ND license (http://creativecommons.org/licenses/by-nc-nd/4.0/).

Keywords Macrophage; GHSR; Meta-inflammation; Macrophage polarization; Insulin resistance; Obesity

1. INTRODUCTION

Obesity-associated chronic inflammation, aka meta-inflammation, has been linked to a wide range of metabolic dysfunctions, such as insulin resistance [1,2], fatty acid dysregulation [3,4], and nonalcoholic fatty liver disease (NAFLD) [5,6]. Macrophages are among the first responders of inflammation, which are the primary responses of metabolic insults [7]. Meta-inflammation increases circulating inflammatory mediators and promotes the recruitment, proliferation, and activation of macrophages into tissues, leading to detrimental outcomes in tissues such as adipose tissue and liver [8—10]. Phenotypic and functional changes of both recruited and resident macrophages have been shown to play critical roles in the local microenvironment and tissue homeostasis [11,12]. Macrophages present a range of polarization states which are defined as either M1-like pro-inflammatory or M2-like anti-inflammatory subtypes, depending on the stimuli [13—15]. M1-

[1]Department of Nutrition, Texas A&M University, College Station, TX 77843, USA [2]Department of Marine Bioindustry, Hanseo University, Seosan 31962, South Korea [3]USDA/ARS Children's Nutrition Research Center, Department of Pediatrics, Baylor College Medicine, Houston, TX 77030, USA [4]Department of Microbial Pathogenesis and Immunology, Texas A&M University Health Science Center, Bryan, TX 77807, USA [5]Agilent technologies, Aanta Clara, CA 95051, USA [6]Texas A&M Institute for Genome Sciences and Society, Department of Cell Biology and Genetics, Texas A&M University, College Station, TX 77843, USA [7]Department of Veterinary Pathobiology, Texas A&M University, College Station, TX 77843, USA [8]Tlaloc Therapeutics Inc., College Station, TX 77845, USA

[9] These authors contributed equally.

*Corresponding author. Department of Nutrition, Texas A&M University, College Station, TX 77843, USA. E-mail: Yuxiang.Sun@tamu.edu (Y. Sun).

List of abbreviation

Arg1	arginase 1
Atgl	adipose triglyceride lipase
B3ar	beta-3 adrenoceptor
BAT	brown adipose tissue
BMDMs	bone marrow-derived macrophages
CCR2	C—C chemokine receptor type 2
CLS	crown-like structure
CM	conditioned media
DIO	diet-induced obesity
eWAT	epididymal white adipose tissue
FAO	fatty acid oxidation
FFAs	free fatty acids
GHSR	growth hormone secretagogue receptor
GPCR	G-protein coupled receptor
H&E	hematoxylin and eosin
HFCS	high fructose corn syrup
HFD	high-fat diet
HOMA-IR	homeostatic model assessment for insulin resistance
Hsl	hormone-sensitive lipase
IL	interleukin
IMs	infiltrating macrophages
iNOS	inducible nitric oxide synthase
IR	insulin receptor
IRS2	insulin receptor substrate 2
iWAT	inguinal fat
KCs	Kupffer cells
LAMs	lipid-associated macrophages
Lgals3	lectin, galactose binding, soluble 3
Lipa	lysosomal acid lipase A
Lpl	lipoprotein lipase
LPS	lipopolysaccharide
MCP1	monocyte chemoattractant protein 1
M-CSF	macrophage colony-stimulating factor
MFI	median fluorescence intensity
Mmp12	matrix metallopeptidase 12
NAFLD	nonalcoholic fatty liver disease
NASH	nonalcoholic steatohepatitis
NF-κB	nuclear factor-kappa B
OCR	oxygen consumption rate
PA	palmitic acids
PBMC	peripheral blood mononuclear cell
PKA	protein kinase A
PMs	peritoneal macrophages
PPAR	peroxisome proliferator-activated receptor
Prkaca	protein kinase cAMP-activated catalytic subunit alpha
RD	regular diet
RMs	resident macrophages
siRNA	small interfering RNA
SVF	stromal vascular fraction
TNFα	tumor necrosis factor α

like macrophages express F4/80 and CD38 but not CD206, producing pro-inflammatory cytokines/enzymes such as tumor necrosis factor α (TNFα), interleukin1β (IL1β), IL6, and inducible nitric oxide synthase (iNOS) [16,17]. In contrast, M2-like macrophages express F4/80 and CD206, but not CD38, thus releasing anti-inflammatory cytokines such as IL10 and arginase 1 (Arg1) [13,14]. The M1-like:M2-like macrophage ratio has been used as an indicator of inflammation state.

Growth hormone secretagogue receptor (GHSR), the receptor of orexigenic hormone ghrelin and a G-protein coupled receptor (GPCR), is known to mediate ghrelin's effects on appetite stimulation and promotion of obesity/insulin resistance [18−22]. We and others found that GHSR is highly expressed in the brain (highest in the hypothalamus), but much lower expression levels in peripheral tissues [21,23]. Our recent study showed that neuronal *Ghsr* deletion negates diet-induced obesity (DIO) by regulating centrally controlled thermogenesis [24]. The second highest expression of GHSR is detected in immune cells, including macrophages and monocytes [14,25]. We have reported that global *Ghsr* ablation promotes an anti-inflammatory shift in peritoneal macrophages (PMs) and adipose tissue macrophages in aging mice [14]. We also showed that global *Ghsr* ablation mitigates high fructose corn syrup (HFCS)-induced adipose inflammation and nonalcoholic steatohepatitis (NASH) [26]. Our *in vitro* data also showed that antagonism of GHSR decreases gene expression of pro-inflammatory cytokines in macrophage cell line RAW264.7 cells [14], indicative of a cell-autonomous effect of GHSR in macrophages. These exciting observations collectively suggest that GHSR has a cell-autonomous effect in macrophages, and GHSR likely plays a critical role in macrophage programming. However, no study has investigated the cell-specific role of GHSR in macrophages. While ample literature in the last 20 years shows that nutrient-sensing ghrelin signaling has paramount importance in metabolism, its role in immunity is largely unexplored. In this study, we aim to determine the macrophage-specific role of GHSR in meta-inflammation and its associated metabolic dysfunctions. To determine the direct effect of GHSR in macrophages, we generated myeloid-specific *Ghsr*-deleted mice (*LysM-Cre;Ghsr^{f/f}*). Excitingly, we found that myeloid-specific *Ghsr* deficiency significantly attenuated diet-induced meta-inflammation and insulin resistance. High-fat diet (HFD)-fed *LysM-Cre;Ghsr^{f/f}* mice showed reduced macrophage infiltration and inflammation in both epididymal white adipose tissue (eWAT) and liver. Furthermore, *Ghsr* deficiency mitigates pro-inflammatory macrophage polarization through the PKA-CREB-IRS2-AKT2 signaling pathway. To our knowledge, this is the first time, nutrient-sensing ghrelin signaling is linked to immune regulation and meta-inflammation. GHSR is a GPCR that is a highly desirable drug target. Thus, our findings may have profound implications for the understanding of immunometabolism and disease prevention/treatment.

2. MATERIAL AND METHODS

2.1. Animals

We previously reported the generation of fully backcrossed *Ghsr* floxed mice on C57BL/6J background [24]. Using a Cre-Lox system, we generated myeloid-specific *Ghsr*-deficient (*LysM-Cre;Ghsr^{f/f}*) mice by breeding fully backcrossed *Ghsr^{f/f}* mice with widely used myeloid-specific *LysM-Cre* mice (JAX stock 4781) [27]. Mice were housed in the animal facility of Texas A&M University (College Station, TX), and maintained on 12-hour light and 12-hour dark cycles (lights on at 6:00 AM and off at 6:00 PM) at an ambient temperature of 75 ± 1 °F. Food and water were available *ad libitum*. All diets were obtained from Harlan Teklad with the following composition by calories: RD (diet

2018) with 18% fat, 58% carbohydrates, 24% protein; HFD (TD 88137) with 42% fat, 42.7% carbohydrates, 15.2% protein calories.

2.2. Body composition, indirect calorimetry, and functional tests

All body composition, food intake, physical activity, energy expenditure, glucose tolerance tests, and insulin tolerance tests were performed as we previously described [21].

2.3. Blood chemistry analysis

Blood was collected by retroorbital bleeding during anesthesia. The blood samples were allowed to clot at room temperature for 30 min before centrifugation (20,000 g, 4 °C, 15 min), then the serum was collected and stored at −80 °C until analysis. Plasma insulin was measured using RIA assay kit (Millipore-Sigma, Billerica, MA). Adipokine and cytokine levels were measured using a commercially available mouse adipokine kit (Millipore-Sigma, Billerica, MA) with Luminex reader, according to the manufacturer's instructions. Serum adiponectin and FFA were analyzed using adiponectin ELISA kit (Millipore-Sigma, Burlington, MA) and FFA ELISA kit (Cayman Chemical, Ann Arbor, MI), respectively. Serum AST and ALT were measured using DxC 700 AU Chemistry Analyzer (Beckman Coulter, Brea, CA).

2.4. Peripheral blood mononuclear cell isolation and flow analysis

Peripheral blood was collected from submandibular vein (cheek punch) using EDTA-coated Mini Collect tubes (Greiner Bio-One, Kremsmünster, Austria). For each sample, 50 μl of whole blood was analyzed for myeloid cell immunophenotyping. For flow cytometry analysis, cells were prepared as described previously [28]. Cells were pre-incubated with anti-FcγR II/III antibody (BD Bioscience, San Jose, CA) for 15 min on ice, followed by 30 min incubation on ice with BV510 anti-mouse CD45 antigen (Biolegend, San Diego, CA), eFluor450 anti-mouse CD11b antigen (Thermo Fisher Scientific, Waltham, MA), APC anti-mouse Ly6C antigen (Thermo Fisher Scientific, Waltham, MA), BV785 anti-mouse Ly6G antigen (Biolegend, San Diego, CA), APC-eFluor780 anti-mouse CD115 antigen (Thermo Fisher Scientific, Waltham, MA), PE anti-mouse CX3CR1 antigen (Biolegend, San Diego, CA), and FITC anti-mouse CCR2 antigen (Biolegend, San Diego, CA). After the staining with surface markers, red blood cells were lysed with FACS Lysing solution (BD Bioscience, San Jose, CA), followed by cell fixation in 2% PFA on ice for 30 min. Calibration was performed using antibody-conjugated CompBeads (BD Bioscience, San Jose, CA). Cells were analyzed on a Fortessa X-20 (BD Bioscience, San Jose, CA). Analyses were performed using FlowJo software v10.

2.5. Isolation and flow cytometry analysis of SVF of eWAT and non-parenchymal cells of liver

SVF of eWAT was isolated as described previously [29,30]. Briefly, 500 mg of eWAT was dissected and minced in RPMI 1640 media containing 1 mg/ml collagenase Type I (Worthington Chemicals, Lakewood, NJ). The solution was incubated in 37 °C water bath for 30 min. The tissue slurry was then filtered through nylon mesh to remove undigested tissue and centrifuged at 2,200×g to fractionate adipocytes and SVF.

Liver NPCs were isolated as described previously [31]. Briefly, a 20G catheter was put through the mouse superior vena cava, the inferior vena cava was clamped, and the portal vein was cut while infusing with HBSS buffer (Calcium-free HBSS containing 0.5 mM EGTA and 5.5 mM glucose, 1% Penicillin−Streptomycin, pH 7.4). After the color of liver changed to light brown, buffer was changed to a digestion buffer (HBSS with 1.5 mM calcium, 0.5 mg/ml type II collagenase, 5.5 mM glucose, 1% P/S, pH 7.4). Cells from digested liver were resuspended in ACD solution (1× HBSS, supplemented with 0.5% FBS, 0.6% citrate-dextrose solution, and 10 mM HEPES), passed through a 100 μm cell strainer, and fractionated using 30% (w/v) Nycodenz (Axis-Shield PoC AS, Oslo, Norway) at 1.155 g/ml to yield liver NPCs, and were then further purified using 30% Percoll (Millipore-Sigma, Burlington, MA) at 1.04 g/ml.

Collected SVF cells and NPCs (1 × 10^6 in a volume of 100 μl of PBS) were washed twice with FACS buffer (PBS, pH 7.4, with 2% FBS) and incubated with anti-FcγR II/III antibody (BD Bioscience, San Jose, CA) for 15 min on ice to assess background fluorescence, and then stained for 30 min on ice with a mixture of fluorescently-labeled antibodies against surface markers such as BV510 anti-mouse CD45 antigen (Biolegend, San Diego, CA), Alexa Fluor 700 anti-mouse Ly6G antigen (Biolegend, San Diego, CA), APC-cy7 anti-mouse CD11b antigen (Biolegend, San Diego, CA), PE-cy7 anti-mouse F4/80 antigen (eBioscience San Diego, CA), and BV421 anti-mouse CX3CR1 antigen (Biolegend, San Diego, CA). Cells were washed and stained with 7AAD (BD Bioscience, San Jose, CA) before data acquisition on a MoFlo Astrios EQ (Beckman Coulter Life Sciences, Indianapolis, IN). Data was analyzed using FlowJo software (Tree Star Inc., Ashland, OR).

2.6. Immunohistochemistry staining

eWAT and liver sections were stained with H&E, Oil-Red-O (Thermo Fisher Scientific, Waltham, MA), or immuno-stained with antibody against Mac-2 (Abcam, Cambridge, UK) according to routine immunohistochemistry protocols [14,21,26]. Adipocyte diameter in eWAT sections were analyzed using image J software (Tree Star Inc., Ashland, OR).

2.7. PM isolation

PMs were obtained from the peritoneums of the mice as described previously [32]. Briefly, mice were euthanized by rapid cervical dislocation after anesthetization with isoflurane. Then, 3 ml of ice-cooled PBS with 2% FBS was injected into abdominal cavity. After gentle shaking for 3 min, abdominal fluid was collected into tubes using a syringe with 18G needle. Red blood cells were lysed with ACK lysis buffer for 5 min and the reaction stopped by adding two times volume of PBS. PMs were then collected for mRNA (1.5 × 10^6) and flow cytometry (2 × 10^5 cells/well).

2.8. Bone marrow-derived macrophages (BMDM) isolation and culture

Bone marrow cells were isolated from the tibias and femurs of mice as described previously [33]. Cells were seeded into 6-well plates at a density of 1.5 × 10^6 cells/well and cultured in a humidified incubator at 37 °C and 5% CO₂ for 7 days. The culture medium was RPMI 1640 medium containing l-glutamine, 10% FBS, 100 U/ml penicillin/streptomycin, and supplemented with 10 ng/ml macrophage colony-stimulating factor (M-CSF). At the end of the 7 days culture period, >95% of the cells were positive for macrophage markers, and the BMDMs were then subjected to inflammatory stimuli such as PA (150 μM) or LPS (100 ng/ml) for further analysis.

2.9. Flow cytometry of PMs and BMDMs

Collected PMs and BMDMs were washed twice with PBS and stained with live/dead aqua (Thermo Fisher Scientific, Waltham, MA) for 30 min on ice. Cells were then washed with FACS buffer and incubated with anti-FcγR II/III antibody (BD Bioscience, San Jose, CA) for 15 min. PMs were subsequently stained for 30 min on ice with a mixture of fluorescently-labeled antibodies against surface markers such as PerCP anti-mouse CD45 antigen (BD Bioscience, San Jose, CA), Alexa

Fluor 700 anti-mouse Ly6G antigen (Biolegend, San Diego, CA), APC-cy7 anti-mouse CD11b antigen (Biolegend, San Diego, CA), PE-cy7 anti-mouse F4/80 antigen (eBioscience, San Diego, CA), PE anti-mouse CD38 antigen (BD Bioscience, San Jose, CA), and Alexa Fluor 488 anti-mouse CD206 antigen (Biolegend, San Diego, CA). BMDMs were stained with a mixture of fluorescently labeled antibodies against surface markers such as APC-cy7 anti-mouse CD11b antigen (Biolegend, San Diego, CA), PE-cy7 anti-mouse F4/80 antigen (eBioscience, San Diego, CA), and PE anti-mouse CD38 antigen (BD Bioscience, San Jose, CA). PMs were further washed and permeabilized for 30 min on ice. Intracellular markers such as TNFα, IL1β, IL6, and iNOS were further stained for 30 min on ice with PE-Dazzle594 anti-mouse TNFα antigen (Biolegend, San Diego, CA), PE anti-mouse IL1β antigen (Thermo Fisher Scientific, Waltham, MA), APC anti-mouse IL6 antigen (BD Bioscience, San Jose, CA), and Alexa Fluor488 anti-mouse iNOS antigen (Thermo Fisher Scientific, Waltham, MA), respectively. Finally, cells were washed before data acquisition on a MoFlo Astrios EQ (Beckman Coulter Life Sciences, Indianapolis, IN) and analyzed using FlowJo software (Tree Star Inc., Ashland, OR).

2.10. Seahorse analysis of glycolysis and mitochondrial oxidative phosphorylation

For Seahorse extracellular flux (XF) analysis, BMDMs were stimulated with 150 μM of XF Palmitate-BSA FAO substrate (Seahorse Bioscience, North Billerica, MA, USA) for 24 h for Seahorse XF Palmitate Oxidation Stress test, 100 ng/ml of LPS for 24 h for Seahorse XF Glycolytic Rate Assay, and primary hepatocytes treated with BMDM conditioned media (CM) for 24 h for Seahorse XF mitochondrial stress test. OCR and ECAR of cells were monitored. The experiments were performed according to the manufacturer's protocol (#102720-100, #103344-100, and #103015-100, Seahorse Bioscience) as described previously [34,35]. Results were analyzed using XFe Wave software (Seahorse Bioscience). The number of cells in each well was measured using a DNA-based stain (CyQUANT Cell Proliferation Assay Kit, Invitrogen) to normalize the data.

2.11. NF-κB nuclear translocation immunostaining and image analysis

NF-κB translocation was measured as described previously [36], with minor modifications. BMDMs were cultured on a coverslip in a 35 mm dish at about 70% confluency. Cells were treated with LPS (100 ng/ml) for 45 min, and cells were then washed twice with DPBS and fixed with 4% paraformaldehyde for 15 min. After fixation, the cells were washed with DPBS and blocked with protein-free blocking buffer including 0.3% Triton X-100 for 1 h. After blocking, NF-κB p65 antibody (Cat. No. 8242; Cell Signaling Technologies, Danvers, MA, USA) was added to the blocking buffer and incubated overnight at 4 °C. After two DPBS washes, anti-rabbit AF-488 (Cat. No. A11008; Invitrogen) secondary antibody was incubated for 1 h and washed with DPBS, and the cells were then mounted with a mounting medium containing DAPI. Images were taken by ImageStream (Cytek Biosciences, Fremont, CA). More than 8000 counts of each sample were obtained. A similarity score was determined for every cell, based on a pixel-by-pixel correlation of the nuclear image to the NF-κB image using IDEAS image analysis software (MilliporeSigma, Burlington, MA). The mean similarity values were generated for each sample.

2.12. siRNA transfection and treatment

Cells were cultured in RPMI 1640 culture medium containing l-glutamine, 10% FBS, 100 U/ml Pen/Strep in a humidified incubator at 37 °C and 5% CO$_2$. The cells were seeded in 6-well plate (1 $\times$ 10^6 cells/well)

and transfected with siRNAs using Lipofectamine 3000 (Invitrogen, Waltham, MA). 100 pmol of *Prkaca* siRNA, *Irs2* siRNA, and control siRNA (Thermo Fisher Scientific, Waltham, MA) were transfected for 18 h in OPTI-MEM. *Prkaca* siRNA transfected cells were applied with 100 ng/ml LPS or 150 μM PA for 4 or 24 h, respectively, for gene expression analysis. *Irs2* siRNA transfected cells were applied with 10 ng/ml LPS for 30 min for protein expression analysis.

2.13. Plasmid transfection

The plasmid of pcDNA3.1-*Ghsr* was constructed by cloning the coding region of *Ghsr* into pcDNA3.1 vector (Invitrogen, Waltham, MA) as described previously [37]. RAW264.7 cells were transfected with pcDNA3.1 vector or pcDNA3.1-*Ghsr* plasmid using Lipofectamine 3000 (Invitrogen, Waltham, MA) according to the manufacturer's instruction. After 36 h transfection, cells were treated with either 10 ng/ml LPS or saline. Cells were collected for qPCR and Western blotting analysis.

2.14. Quantitative real-time PCR

Total RNA was isolated using TRIzol® Reagent (Invitrogen, Carlsbad, CA) or Aurum Total RNA mini kit (Bio-Rad Laboratories, Inc., Hercules, CA) according to the manufacturers' instructions [38]. The RNA samples were treated with DNase (Ambion, Austin, TX) to remove genomic DNA. Reverse transcription was performed using Superscript III First Strand Synthesis System (Invitrogen, Carlsbad, CA) according to the manufacturer's instructions. Quantitative real-time PCR reaction was performed as we previously described [39]. Ghsr-1a primers are designed franking the intron to distinguish from Ghsr-1b as below: sense primer 5′-GGACCAGAACCACAAACAGACA-3′, anti-sense primer 5′-CAGCAGAGGATGAAAGCAAACA-3 [40]. The rest of the primer information is available upon request.

2.15. Western blotting

BMDMs (3 $\times$ 10^6 per well in 6-well cell culture plates) or RAW264.7 cells (2 $\times$ 10^6 per well in 6-well cell culture plates) were treated with LPS 10 or 100 ng/ml for 30 min and lysed in RIPA buffer with protease and phosphatase inhibitors (Roche, Nutley, NJ). Western blot analysis was performed with primary antibodies against p-CREB-S133, CREB, IRS1, IRS2, p-AKT-S473, AKT, p-AKT1-S473, AKT1, p-AKT2-S474, AKT2, p-NF-κB P65-S536, NF-κB P65, IκBα, β-actin, and GAPDH from Cell Signaling Technology (Denvers, MA) and GHSR from Invitrogen (Waltham, MA). Signaling was visualized with ECL (Genesee Scientific, San Diego, CA) and analyzed using Image J software.

2.16. Statistical analysis

Statistical analyses were performed with GraphPad Prism 6.01. Data were presented as mean $\pm$ SEM. Student's t-test was used to determine the significance of the difference between two groups. One-way or two-way ANOVA test was used to determine the significance of the differences between multiple groups; $P < 0.05$ was considered significant.

3. RESULTS

3.1. Generation of myeloid-specific *Ghsr*-deficient mice

To investigate the cell-specific role of GHSR in macrophages, we first generated a myeloid-specific *Ghsr*-deficient mouse model by breeding lysozyme (LysM)-Cre mice (JAX stock 4781) with our fully backcrossed *Ghsr$^{f/f}$* mice [24,27,41]. Heterozygous *LysM-Cre;Ghsr$^{f/+}$* mice were used to breed homozygous *LysM-Cre;Ghsr$^{f/f}$* mice as shown in the gene-targeting strategy diagram (Figure S1A). In *LysM-Cre;Ghsr$^{f/f}$*

mice, *Ghsr* expression was significantly decreased (74%) in PMs (Figure S1B). *Ghsr* expression in stromal vascular fraction (SVF) of eWAT that contains immune cells such as macrophages, showed a 57% decrease, but no significant decrease was detected in mature adipocytes of eWAT (Figure S1B). These results suggest that the decrease of *Ghsr* expression is mostly contributed by immune cells such as macrophages, not adipocytes. *Ghsr* expression levels were not changed in the brain (even though GHSR is highly expressed in the brain) nor in other peripheral tissues such as liver and gastrocnemius muscles (Figure S1B). Taken together, these results indicate that *Ghsr* deficiency in *LysM-Cre;Ghsr^{f/f}* mice is restricted to myeloid cells.

3.2. Myeloid-specific *Ghsr* deficiency does not affect metabolic characteristics under homeostatic condition

Under regular diet (RD) feeding for 7 months, control (*Ghsr^{f/f}*) and *LysM-Cre;Ghsr^{f/f}* mice exhibited similar body weight, body fat composition, and tissue weight (Figure S1C—E). Myeloid-specific

Ghsr deficiency had no significant effect on serum active ghrelin levels (Figure S1F) and metabolic profiles, including food intake, physical activity, and energy expenditure (Figure S1G—I). Myeloid-specific *Ghsr* deficiency had no significant effect on glycemic profiles of blood glucose, plasma insulin, glucose tolerance, and insulin sensitivity (Figure S1J—M). These data demonstrate that under RD-fed homeostatic condition, myeloid-specific *Ghsr* deficiency doesn't have a major impact on energy or glucose homeostasis.

3.3. Myeloid-specific *Ghsr* deficiency attenuates diet-induced glucose tolerance and insulin resistance without affecting body weight

Interestingly, we found that *Ghsr* gene expression was dramatically increased in PMs after HFD feeding (Figure 1A), suggesting a potential role of macrophage GHSR in DIO. To examine the role of myeloid-specific GHSR under DIO, we subjected *LysM-Cre;Ghsr^{f/f}* and control
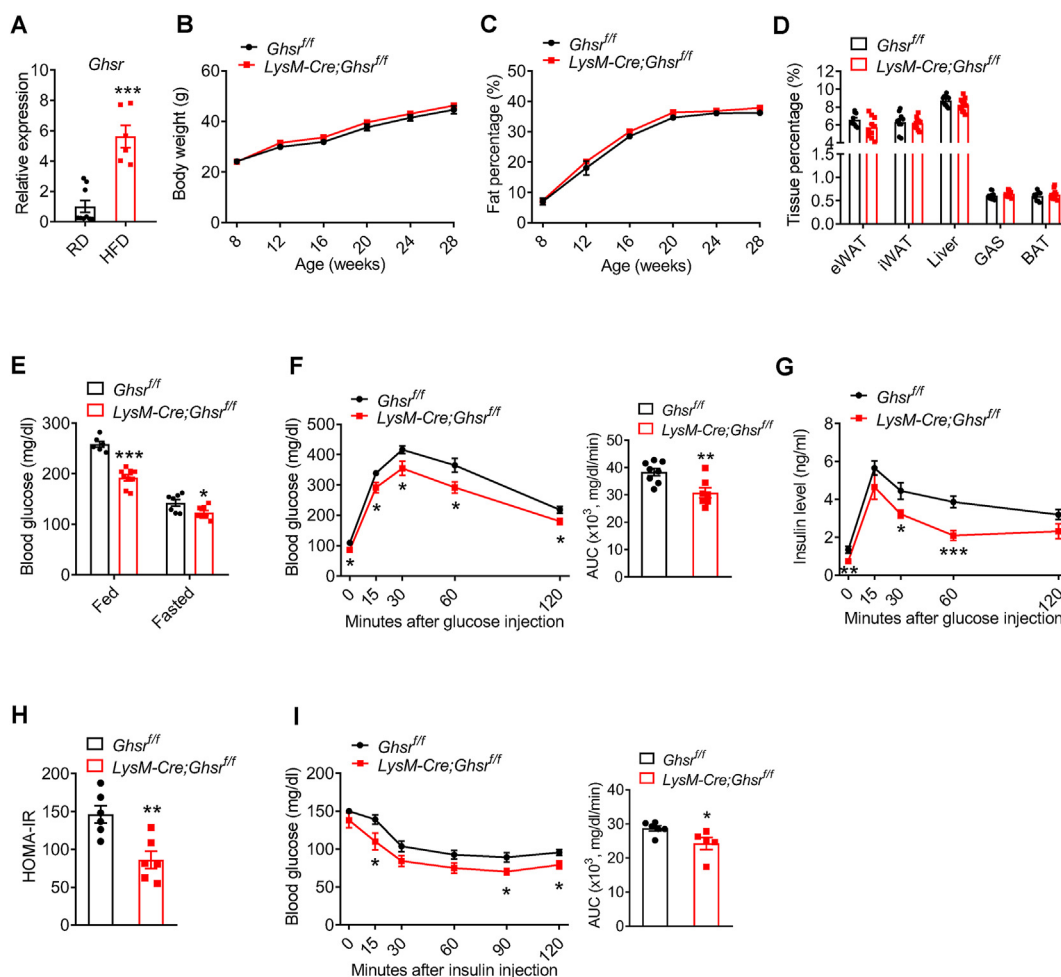

Figure 1: Myeloid-specific *Ghsr* deficiency attenuates diet-induced glucose intolerance and insulin resistance without affecting body weight. Control and *LysM-Cre;Ghsr^{f/f}* mice were fed HFD started from 2 months of age for 5 months. (A) Gene expression of *Ghsr* in PMs of RD-fed and HFD-fed wild-type mice, n = 6—9 mice/group. (B and C) Monthly body weight (B) and fat body composition (C), n = 11—14 mice/group. (D) Percentage ratio of tissue/body weight, n = 9—14 mice/group. (E) Fed and 16 h-fasted blood glucose levels, n = 6—9 mice/group. (F and G) Glucose tolerance test (F) and serum insulin levels during glucose tolerance test (G) after 16 h of overnight fasting, n = 7—10 mice/group. (H) Homeostatic Model Assessment for Insulin Resistance (HOMA-IR) was calculated using the following formula: fasting glucose (mg/dl) $\times$ fasting insulin (ng/ml), n = 6 mice/group. (I) Insulin tolerance test after 6 h of fasting, n = 5—7 mice/group. These experiments were performed on 3 batches of mice. Representative results are shown. Data are presented as the means ± SEM. *$P < 0.05$, **$P < 0.01$, ***$P < 0.001$ by Student's t test (A and E—I), HFD vs. RD or *LysM-Cre;Ghsr^{f/f}* vs. *Ghsr^{f/f}*. n represents the number of biological replicates.

$Ghsr^{f/f}$ mice to a HFD for 5 months started from 2 months of age. The body weight, fat composition, and tissue-to-body weight ratios between control and $LysM$-$Cre;Ghsr^{f/f}$ mice were similar (Figure 1B—D). Myeloid-specific $Ghsr$ deficiency did not alter serum active ghrelin levels, nor did it affect the metabolic profiles of food intake, physical activity, and energy expenditure (Figure S2A—D). Interestingly, myeloid-specific $Ghsr$ deficiency led to 25.6% and 13.6% decrease of blood glucose in fed and 16 hfasted conditions, respectively (Figure 1E). Moreover, $LysM$-$Cre;Ghsr^{f/f}$ mice showed improved glucose tolerance and reduced serum insulin in glucose tolerance tests (Figure 1F and G). Insulin sensitivity was also significantly improved in $LysM$-$Cre;Ghsr^{f/f}$ mice, evident in decreased Homeostatic Model Assessment for Insulin Resistance (HOMA-IR) and enhanced insulin sensitivity in insulin tolerance test (Figure 1H and I). These results reveal that under DIO condition, myeloid-specific $Ghsr$ deficiency protects against diet-induced glycemic dysregulation and insulin resistance.

3.4. Myeloid-specific $Ghsr$ deficiency reduces systemic inflammation under DIO

It is well known that obesity is linked to systemic inflammation, which further triggers systemic and tissue insulin resistance [42,43]. Next, we examined the inflammatory profiles of myeloid-specific $Ghsr$-deficient mice under DIO. Remarkably, compared to HFD-fed control mice, HFD-fed $LysM$-$Cre;Ghsr^{f/f}$ mice showed significantly lower levels of serum pro-inflammatory cytokines/chemokines, such as TNFα, IL1β, IL6, and monocyte chemoattractant protein 1 (MCP1), but with similar levels of serum anti-inflammatory cytokines such as IL4 and IL10 (Figure 2A). These results indicate that myeloid-specific GHSR plays an important role in the pathogenesis of diet-induced meta-inflammation.

C—C chemokine receptor type 2 (CCR2), chemokine receptor of CCL2/MCP1, is known to promote the migration of monocytes into inflamed tissues where they differentiate into M1 pro-inflammatory macrophages and release pro-inflammatory cytokines [44—46]. To further
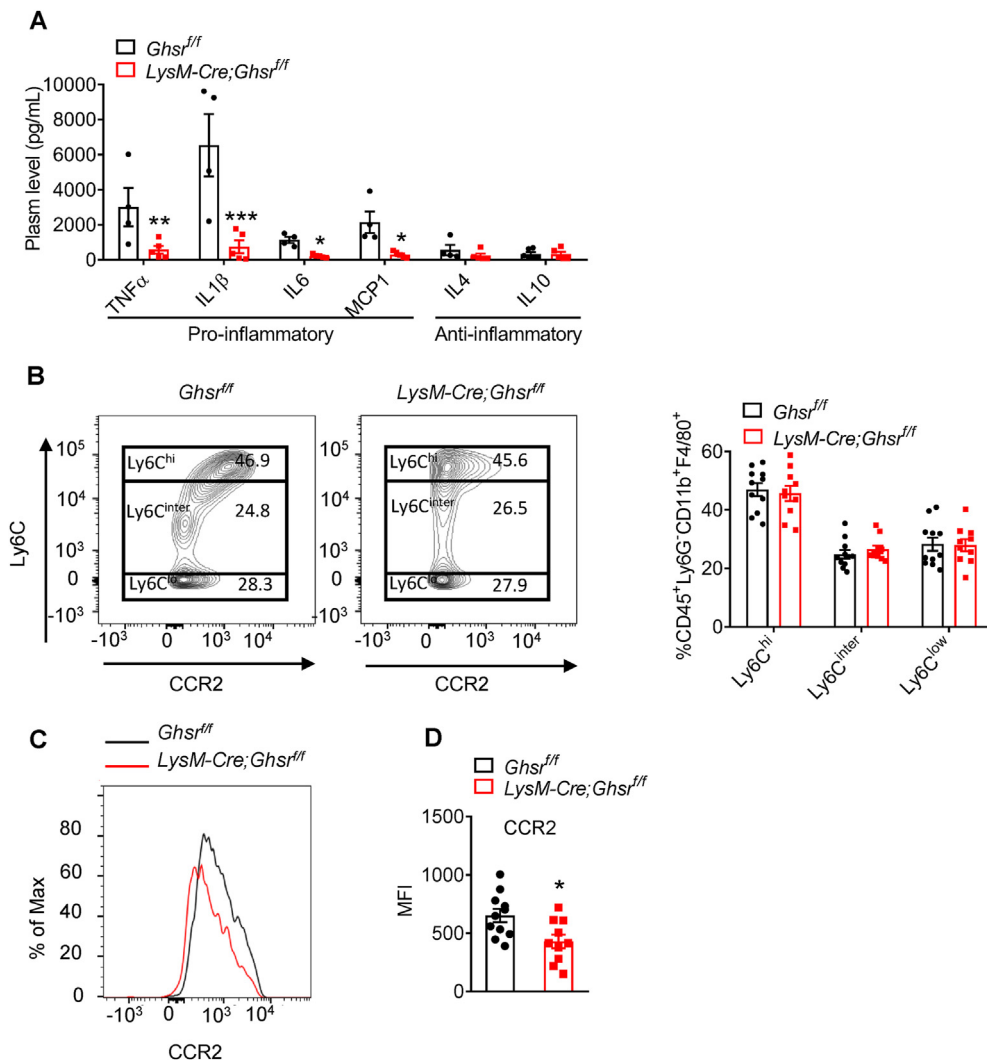

Figure 2: Myeloid-specific $Ghsr$ deficiency reduces systemic inflammation under DIO. Control and $LysM$-$Cre;Ghsr^{f/f}$ mice were fed HFD started from 2 months of age for 5 months. (A) Serum inflammatory cytokine levels, n = 4—6. (B) Percentage of Ly6C^{hi}, Ly6C^{inter}, and Ly6C^{low} cells in monocyte subset of PBMCs (CD45$^+$CD11b$^+$CD115$^+$Ly6G$^−$), n = 10—11 mice/group. (C) Representative histograms indicating the percentage of CCR2 determined in Ly6C^{hi} monocyte subset of PBMC by flow cytometry. (D) Median fluorescence intensity (MFI) of CCR2 expression in pro-inflammatory monocyte subset (CD45$^+$CD11b$^+$CD115$^+$Ly6G$^−$Ly6C^{hi}). These experiments were performed in 2 batches of mice. Representative results are shown. Data are presented as the means ± SEM. *$P < 0.05$, **$P < 0.01$, ***$P < 0.001$ by Student's t test (A and D), $LysM$-$Cre;Ghsr^{f/f}$ vs. $Ghsr^{f/f}$. n represents the number of biological replicates.

investigate the effect of myeloid-specific GHSR on monocyte programming under meta-inflammation, peripheral blood mononuclear cell (PBMC) subsets were characterized by multichannel flow cytometry as described previously [47]. Gating strategy was shown in Figure S3A−C. Briefly, PBMCs were labeled with fluorescence-tagged antibodies CD45, CD11b, CD115, and Ly6G to identify the monocyte population (CD45$^+$CD11b$^+$CD115$^+$Ly6G$^-$). Monocyte subsets of Ly6C^{hi}, Ly6C^{inter} or Ly6C^{lo} were further examined, Ly6C^{hi} and Ly6C^{lo} gated monocytes were defined as pro-inflammatory and patrolling monocytes, respectively [48−50]. We found that the percentage of Ly6C^{hi} subset monocytes was comparable between genotypes (Figure 2B), whereas the expression of CCR2 in Ly6C^{hi} was reduced in PBMCs of HFD-fed *LysM-Cre;Ghsr$^{f/f}$* mice, evident in a significant decrease in the percentage of max (normalized CCR2 expression with the cell counts) and median fluorescence intensity (MFI) (Figure 2C and D). These results demonstrate that *Ghsr* deficiency in myeloid cells decreases CCR2 expression in monocytes, which leads to reduced migration of pro-inflammatory monocytes.

3.5. Myeloid-specific *Ghsr* deficiency attenuates obesity-associated macrophage infiltration and inflammatory response in eWAT

Monocyte CCL2-CCR2 is known to regulate the migration of monocytes to the site of inflammation in the inflamed tissues [46]. The PBMC results suggest that GHSR may affect monocyte infiltration. We next investigated the effect of myeloid-specific *Ghsr* deficiency on obesity-associated macrophage infiltration and inflammation in adipose tissues. We found that percentages of crown-like structure (CLS) and Mac-2 positive cells were markedly reduced in eWAT of HFD-fed *LysM*-Cre;*Ghsr$^{f/f}$* mice compared to that of HFD-fed control mice (Figures 3A, B, S4A and B). We also validated the effect of HFD feeding on macrophage infiltration in eWAT using flow cytometry with our established gating strategy (Figure S5A−C). This gating strategy enabled us to distinguish two distinct populations of infiltrating macrophages (IMs) and resident macrophages (RMs) by separating F4/80^{hi} and F4/80^{lo} macrophage populations (Figure S5D). The results clearly demonstrate that HFD feeding significantly increased IM but not RM population in the eWAT of control mice (Figure S5D). In addition, we examined different subsets of myeloid cells, such as neutrophils and macrophages in eWAT. The percentage of total myeloid cell population was significantly increased in eWAT under HFD feeding, mostly due to the increase of macrophages but not neutrophils (Figure S5E). We then tested the effect of *Ghsr* deficiency on percentage of total myeloid cell population in eWAT. Myeloid-specific *Ghsr* deficiency significantly reduced total macrophages in eWAT under HFD feeding while showing a reduced trend in neutrophil percentage (Figure S5F).

It has been shown that CX3CR1 is expressed in monocyte-derived macrophages and exhibits low expression in the RM population [51,52]. We studied CX3CR1 marker in the IM and RM populations in our model. Remarkably, compared to HFD-fed control mice, IM population in eWAT was decreased by 20.3%, while RM population was not significantly affected in HFD-fed *LysM*-Cre;*Ghsr$^{f/f}$* mice (Figure 3C). Consistently, the percentage of CX3CR1$^+$ IM subset in eWAT of HFD-fed *LysM*-Cre;*Ghsr$^{f/f}$* mice was significantly reduced by 34.3%, compared to that of HFD-fed control mice (Figure 3D). The percentage of max intensity normalizing the CX3CR1 expression to the cell count was also decreased in the IM subset of eWAT of HFD-fed *LysM*-Cre;*Ghsr$^{f/f}$* mice, shifting to the left (Figure 3E). In line with the reduced macrophage infiltration in eWAT of HFD-fed *LysM-Cre;Ghsr$^{f/f}$* mice, myeloid-specific *Ghsr* deficiency significantly reduced the expression levels of pro-inflammatory cytokine genes, such as *Tnfa*, *Il1b*, *Il6*, and

Mcp1 in eWAT by 55.7%, 64.1%, 65.3%, and 40.0%, respectively (Figure 3F).

Emerging data from single cell/nuclei RNA-seq studies suggest HFD is associated with more nuanced macrophage classes in adipose tissue [53,54] and liver [55,56]. One predominant class of macrophages named lipid-associated macrophages (LAMs) is found in obese mice and humans expressing specific markers such as Triggering receptor expressed on myeloid cells-2 (*Trem2*), lysosomal acid lipase A (*Lipa*), lectin-galactose-binding-soluble 3 (*Lgals3*), and matrix metallopeptidase12 (*Mmp12*), etc [54,55]. Thus, we have measured gene expression of LAM-related markers of *Trem2, Lipa, Lgals3,* and *Mmp12* in eWAT of HFD-fed myeloid *Ghsr* deficient mice. We found that myeloid-specific *Ghsr* deficiency significantly increased gene expression of *Trem2* and *Lgals3* by 57.3% and 56.1%, respectively, in eWAT under HFD feeding (Figure 3F). These results indicate that myeloid-specific *Ghsr* deficiency promotes LAM signatures in eWAT under DIO, which is in line with the decreased macrophage infiltration and reduced inflammation in adipose tissues.

Meta-inflammation has been shown to be linked to lipid dysregulation, increased adiposity, reduced circulating adiponectin [57−59], and increased serum free fatty acids (FFAs) [60−62]. Indeed, compared with HFD-fed control mice, HFD-fed *LysM-Cre;Ghsr$^{f/f}$* mice had smaller adipocytes in eWAT (Figure 3G and H), which is in line with the improved insulin sensitivity. In addition, serum adiponectin levels were significantly increased by 29.4% (Figure 3I), and serum FFA levels were significantly decreased by 10.3% (Figure S6A) in HFD-fed *LysM-Cre;Ghsr$^{f/f}$* mice. Consistently, myeloid-specific *Ghsr* deficiency significantly reduced the expression levels of lipid metabolic genes, including adipose triglyceride lipase (*Atgl*), hormone-sensitive lipase (*Hsl*), beta-3 adrenoceptor (*B3ar*), *Perilipin*, and lipoprotein lipase (*Lpl*), in the eWAT (Figure S6B), which was consistent with the reduced serum FFAs in HFD-fed *LysM-Cre;Ghsr$^{f/f}$* mice. Collectively, these data demonstrate that myeloid-specific *Ghsr* deficiency improves lipid metabolic profile of eWAT, which likely contributes to the improved insulin sensitivity.

3.6. Myeloid-specific *Ghsr* deficiency attenuates diet-induced NAFLD by attenuating macrophage infiltration and lipid accumulation in liver

Monocyte/macrophage infiltration exacerbates inflammation in liver, which is positively correlated with the progression of NAFLD [63]. Liver macrophages are characterized as IMs and resident Kupffer cells (KCs) based on their gene expression profiles and developmental origins [64−66]. In the literature, cell expression signature of CX3CR1$^+$ has been used as a marker of IMs, and CX3CR1$^-$ has been used as a marker of KCs [67]. The gating strategy shown in Figure S7A enables us to distinguish between IMs and KCs. As expected, HFD feeding significantly increased the percentage of total myeloid cells, which are evident in total macrophages, IMs, and KCs by 146.5%, 242.0%, and 832.9%, respectively, but had no significant effect on neutrophils (Figure S7B and C). Myeloid-specific *Ghsr* deficiency reduced total macrophages in liver, evident in Mac-2 staining in liver sections and cell counts by flow cytometry (Figures 4A and S7D). Our flow cytometry data further revealed that there was a significant reduction of IMs in the livers of HFD-fed *LysM-Cre;Ghsr$^{f/f}$* mice (Figure 4B). In addition, myeloid-specific *Ghsr* deficiency reduced the percentage of CX3CR1$^+$ IMs but not KCs in the liver (Figure 4C). Consistently, myeloid-specific *Ghsr* deficiency significantly decreased gene expression levels of *Tnfa* and *Il6* in the liver by 40.3% and 47.3%, respectively (Figure 4D). In addition, the expression of LAM-related genes such as *Trem2*, *Lipa*, *Lgals3*, and *Mmp12* was significantly increased by 82.4%, 42.3%,
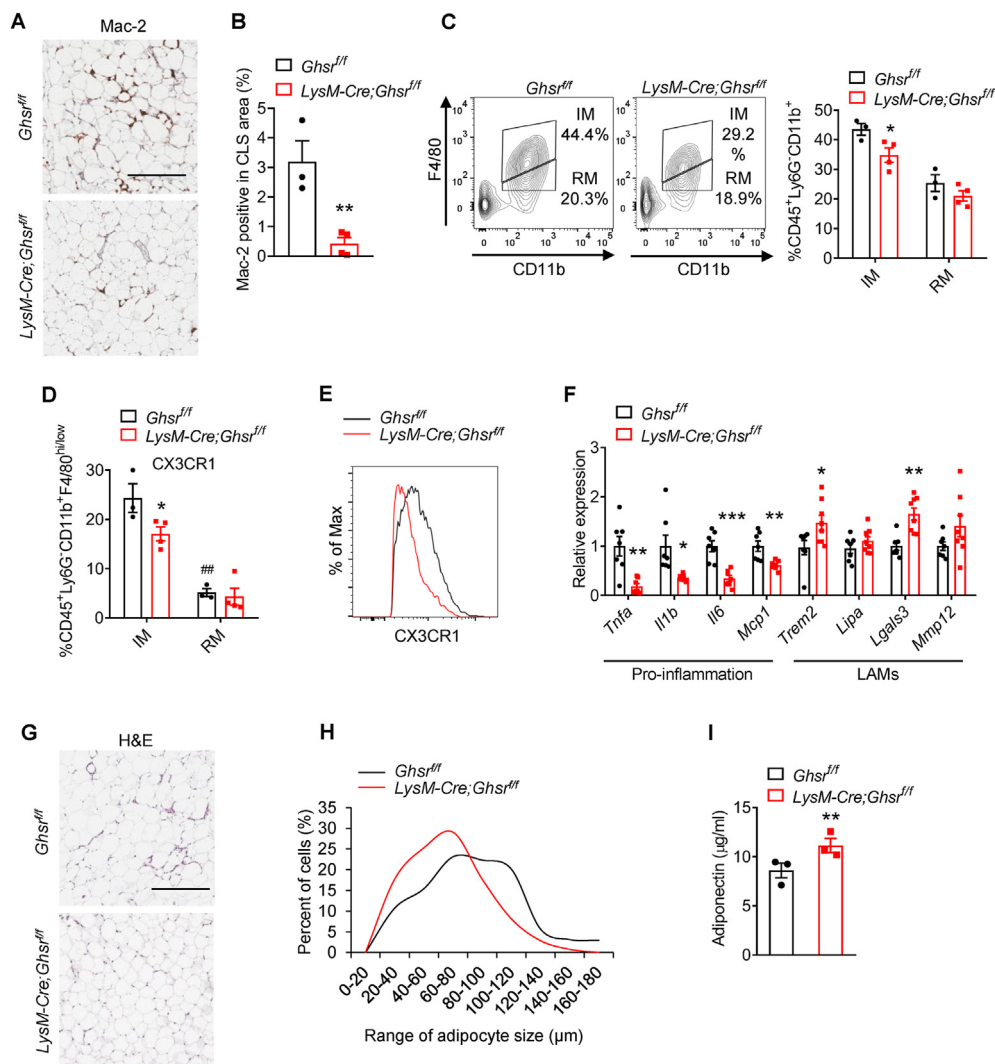
Figure 3: Myeloid-specific *Ghsr* deficiency reduces macrophage infiltration in eWAT of HFD-fed mice. Control and *LysM-Cre;Ghsr^f/f* mice were fed HFD started from 2 months of age for 5 months. (A) Immunohistochemistry staining of Mac-2 in eWAT. Scale bar: 200 μm, n = 3−4 mice/group. (B) Mac-2 positive in CLS area, n = 3−4 mice/group. (C−E) Percentage of infiltrating macrophage subset (IM: CD45⁺Ly6G⁻CD11b⁺F4/80^hi) and resident macrophage subset (RM: CD45⁺Ly6G⁻CD11b⁺F4/80^lo) of adipose tissue macrophages (C), percentage of CX3CR1 in IM and RM population (D), and percentage of max of CX3CR1 from IM (E) in SVF of eWAT, n = 3−4 mice/group. (F) Gene expression of pro-inflammatory cytokine/chemokine- and lipid-associated macrophage (LAM)-related genes in eWAT, n = 7−8 mice/group. (G) Hematoxylin and eosin (H&E) staining of eWAT. Scale bar: 200 μm, n = 3−4 mice/group. (H) Adipocyte size distribution in eWAT, n = 3−4 mice/group. (I) Serum adiponectin levels, n = 3 mice/group. These experiments were performed in 2 batches of mice. Representative results are shown. Data are presented as the means ± SEM. $*P < 0.05$, $**P < 0.01$, $***P < 0.001$, *LysM-Cre;Ghsr^f/f* vs. *Ghsr^f/f*.

44.5%, and 110.4%, respectively, in liver of HFD-fed *LysM-Cre;Ghsr^f/f* mice (Figure 4D).

We further demonstrated that myeloid-specific *Ghsr* deficiency reduced diet-induced liver injury and hepatic steatosis, which are evident in reduced serum alanine transaminase (ALT) and aspartate transaminase (AST) levels, pathological alteration in hematoxylin and eosin (H&E) imaging, and decreased Oil-Red-O staining (Figure 4E and F). In line with the reduced levels of liver damage markers and lipid accumulation, β-oxidation-related genes such as *Ppara* and *Cpt1* were elevated in the livers of HFD-fed *LysM-Cre;Ghsr^f/f* mice by 72% and 80.9%, respectively, compared to HFD-fed control mice (Figure 4G). Next, to determine whether secreting factors of *Ghsr*-deficient macrophages directly affect hepatocytes, we performed a co-culture study using CM. Hepatocytes of wild-type mice were incubated with CM collected from palmitic acids (PA)-treated BMDMs from either control

or *LysM-Cre;Ghsr^f/f* mice. Hepatocytes incubated with CM of PA-treated BMDMs of *LysM-Cre;Ghsr^f/f* mice showed significant increases in *Ppara* and *Cpt1* expression by 26.9% and 22.6%, respectively, as compared to hepatocytes incubated with CM of PA-treated BMDMs of control mice (Figure 4H). To further investigate the functional outcome of β-oxidation state of hepatocytes, we investigated the oxygen consumption rate (OCR) in hepatocytes co-cultured with CM of *Ghsr*-deficient or control BMDMs treated with PA. We found that PA-treated BMDM-CM significantly increased OCR in hepatocytes (Figure 4I). The basal and maximal respiration rates were significantly increased in hepatocytes co-cultured with PA-treated BMDM-CM of *Ghsr*-deficient BMDMs compared to that of control BMDMs, showing 19.6% and 35.9% increase, respectively (Figure 4I). Taken together, these results suggest that *Ghsr* deficiency in macrophages promotes β-oxidation and reduces lipid accumulation in liver.
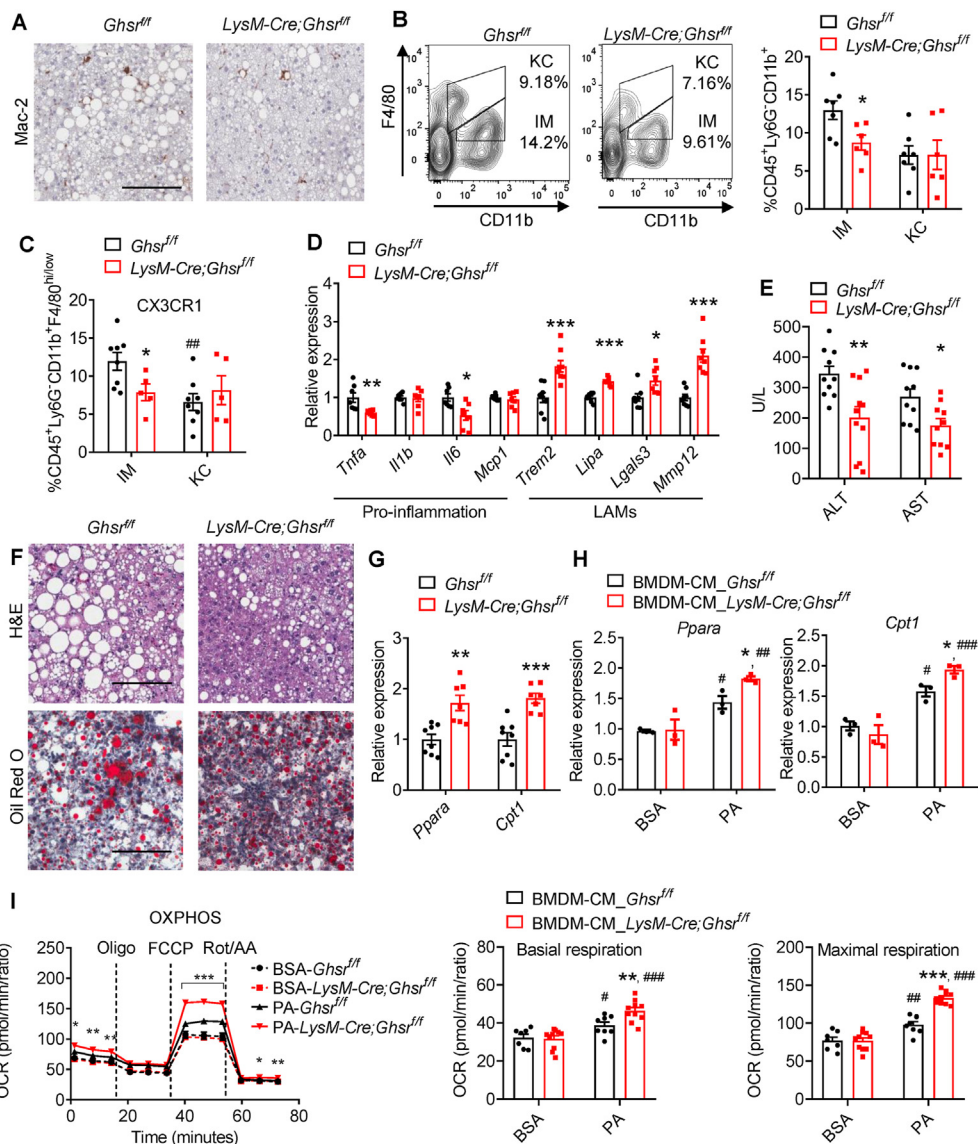
Figure 4: Myeloid-specific *Ghsr* deficiency reduces macrophage infiltration and lipid accumulation in liver of HFD-fed mice. Control and *LysM-Cre;Ghsr*$^{f/f}$ mice were fed HFD started from 2 months of age for 5 months. (A) Immunohistochemistry staining of Mac-2 in liver. Scale bar: 200 µm, n = 3 mice/group. (B and C) Percentage of IM subset (CD45$^+$Ly6G$^-$CD11b$^+$F4/80^{lo}) and KC subset (CD45$^+$Ly6G$^-$CD11b$^+$F4/80^{hi}) of liver macrophages (B), percentage of CX3CR1 in IM and KC population (C) in NPCs of liver, n = 4−5 mice/group. (D) Gene expression of pro-inflammatory cytokine/chemokine- and LAM-related genes in liver, n = 7−9 mice/group. (E) Serum ALT and AST levels, n = 10−11 mice/group. (F) H&E and Oil-red-O staining in liver. Scale bar: 200 µm, n = 3 mice/group. (G) Gene expression of β-oxidation-related genes in liver, n = 7−8 mice/group. (H) Gene expression of β-oxidation-related genes in RD-fed control-hepatocytes incubated with conditioned media (CM) from 150 µM palmitic acid (PA)-treated bone marrow-derived macrophages (BMDMs), n = 3 biological replicates/group. (I) Oxidative phosphorylation (OXPHOS) was measured as oxygen consumption rate (OCR) in hepatocytes co-cultured with PA-treated BMDMs of control and *LysM-Cre;Ghsr*$^{f/f}$, n = 7−10/group. These experiments were performed on 2 batches of mice. Representative results are shown. Data are presented as the means ± SEM. *$P < 0.05$, **$P < 0.01$, ***$P < 0.001$, *LysM-Cre;Ghsr*$^{f/f}$ vs. *Ghsr*$^{f/f}$, #$P < 0.05$, ##$P < 0.01$, ###$P < 0.001$ PA vs. BSA.

3.7. Myeloid-specific *Ghsr* deficiency mitigates HFD-induced pro-inflammatory polarization of PMs

To further assess the direct effect of GHSR on macrophages, PMs were obtained from the peritoneum of HFD-fed control and *LysM-Cre;Ghsr*$^{f/f}$ mice. Flow cytometry gating strategy was shown in Figure S8A and B. PMs were labeled with fluorescence-tagged antibodies CD45, Ly6G, CD11b, and F4/80 for the identification of macrophages (CD45$^+$Ly6G$^-$CD11b$^+$F4/80$^+$). CD38 is recognized as a distinctive marker for M1-like macrophages and CD206 for M2-like macrophages [68,69]. Intracellular expression of TNFα, IL1β, IL6, and iNOS was also gated in the specific subtypes of macrophages. While the percentages

of total myeloid cells and neutrophils were unchanged, HFD feeding significantly increased the macrophage population in PMs compared to RD feeding (Figure S8C). In addition, MFI of CD38 was significantly increased by 175.5%, while MFI of CD206 in macrophage subset remained the same in PMs under HFD feeding (Figure S8D). These results indicate that HFD feeding increases macrophage population in abdominal cavity, and the elevated cells are predominantly M1-like macrophages.

In HFD-fed *LysM-Cre;Ghsr*$^{f/f}$ mice, the percentage of the total myeloid cells, neutrophils, and macrophage populations in peritoneal fluid did not show a significant difference, compared to that of control mice
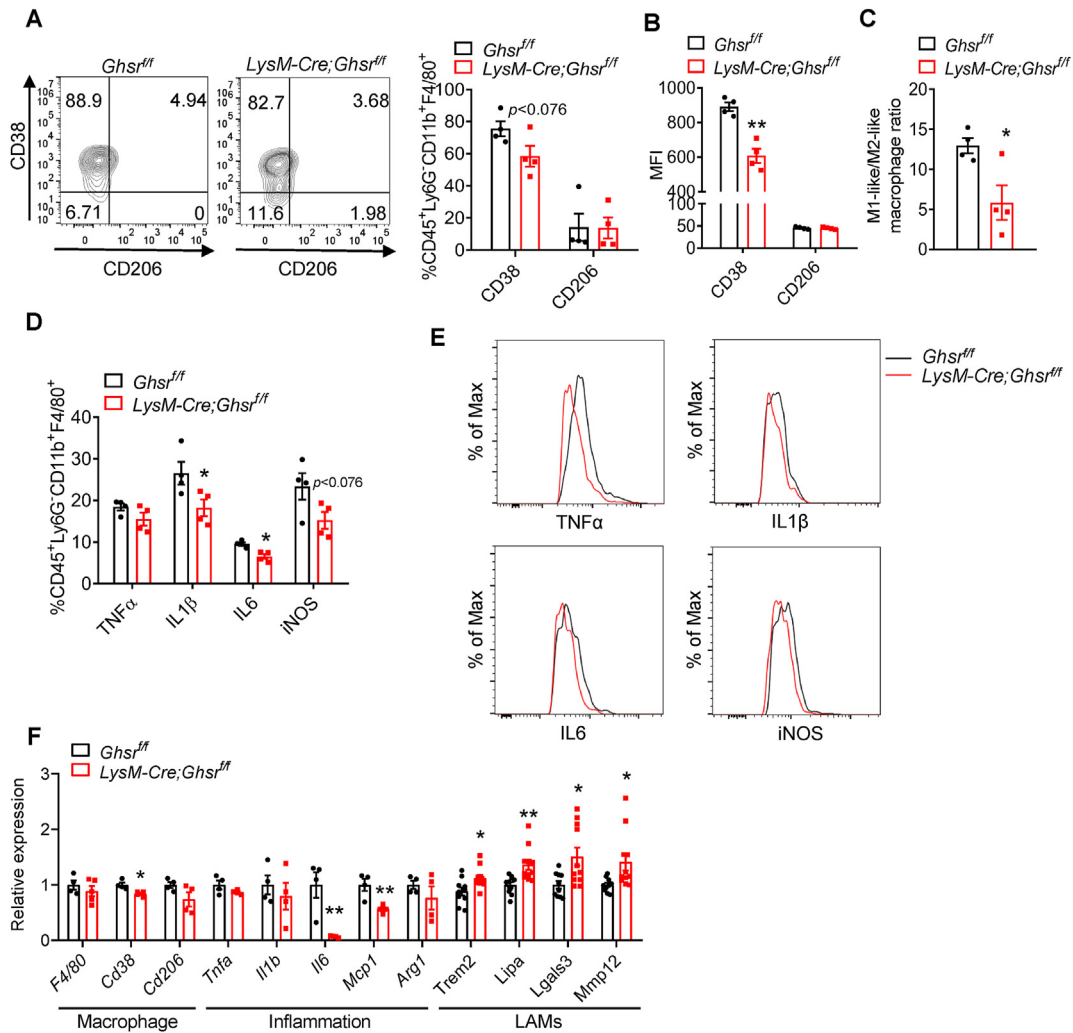
Figure 5: Myeloid-specific *Ghsr* deficiency attenuates HFD-induced inflammatory responses showing reducing M1 polarization in PMs. Control and *LysM-Cre;Ghsr^{f/f}* mice were fed HFD started from 2 months of age for 5 months. (A and B) Percentage (A) and MFI (B) of CD38^+ and CD206^+ in macrophage subset of PMs, n = 4 mice/group. (C) Ratio of M1-like/M2-like macrophages in PMs, n = 4 mice/group. (D and E) Percentage of pro-inflammatory cytokines (D) and percentage of max (E) in macrophage subset of PMs, n = 4 mice/group. (F) Expression of macrophage-, inflammation-, and LAM-related genes in PMs, n = 4−11/group. These experiments were performed on 2 batches of mice. Representative results are shown. Data are presented as the means ± SEM. *$P < 0.05$, **$P < 0.01$, ***$P < 0.001$ *LysM-Cre;Ghsr^{f/f}* vs. *Ghsr^{f/f}*.

(Figure S8E). Interestingly, in PMs, while the cell percentage and MFI of CD206 in the macrophages were unchanged, myeloid-specific *Ghsr* deficiency led to a decreased trend in CD38^+ macrophage population and significantly decreased MFI of CD38 by 31.8% (Figure 5A and B). Moreover, we found a significant reduction in M1-like/M2-like macrophage ratio in PMs of HFD-fed *LysM-Cre;Ghsr^{f/f}* mice (Figure 5C), indicative of a polarization shift toward an anti-inflammatory state. More importantly, our data revealed that PMs of HFD-fed *LysM-Cre;Ghsr^{f/f}* mice have a significant decrease in pro-inflammatory cytokines of IL1β and IL6 by 31.3% and 31.6%, respectively, as well as a reduced percentage of max, the intensity of the cytokine markers normalized to the cell count (Figure 5D and E). Accordingly, the gene expression of pro-inflammatory cell surface and intracellular markers such as *Cd38*, *Il6*, and *Mcp1* were significantly reduced in the PMs of HFD-fed *LysM-Cre;Ghsr^{f/f}* mice by 16.2%, 93.1%, and 46.6%, respectively (Figure 5F). In addition, LAM-related gene expression such as *Trem2*, *Lipa*, *Lgals3*, and *Mmp12* was significantly increased by 22.6%, 36.3%, 51.0%, and 41.6%,

respectively, in PMs of HFD-fed *LysM-Cre;Ghsr^{f/f}* mice (Figure 5F). These results indicate that myeloid-specific *Ghsr* deficiency mitigates HFD-induced pro-inflammatory M1 polarization of PMs and promotes LAM signatures in PMs, underscoring that GHSR is a major pathogenic contributor of phenotypes of macrophage pro-inflammatory polarization and LAM expansion under DIO.

3.8. *Ghsr* deficiency attenuates pro-inflammatory responses in bone marrow-derived macrophages (BMDMs)

To further validate our *in vivo* phenotypic findings and gain mechanistic insights, we sought to assess GHSR-mediated macrophage programming in a controlled *ex vivo* system of BMDMs. BMDMs were treated with PA to mimic the HFD condition to assess BMDM polarization using the gating strategy described in Figure S8A and B. BMDMs were labeled with fluorescence-tagged antibodies CD11b, F4/80, and CD38 for identification of M1-like macrophages. In control BMDMs, PA treatment robustly increased the percentage of CD38^+ macrophage subset and the expression of pro-inflammatory genes, such as *Tnfa*,

Il1b, and *Il6* by 59.6%, 571.4%, and 128.2%, respectively, compared to the BSA-treated control group (Figure S9A and S9B). Strikingly, PA-treated *Ghsr*-deficient BMDMs showed significantly decreased CD38$^+$ macrophage subset (by 44.4%) and reduced expression of pro-inflammatory genes of *Tnfa* (by 38.4%) and *Il1b* (by 59.6%), compared to PA-treated control BMDMs (Figure S9A and S9B). We further tested the effect of *Ghsr* deficiency on exotoxin lipopolysaccharide (LPS)-induced pro-inflammation in BMDMs. The LPS-treated BMDMs from *LysM-Cre;Ghsr^f/f^* mice showed significantly decreased expression of pro-inflammatory genes, such as *Tnfa*, *Il1b*, and *Il6* by 22.3%, 36.8%, and 48.9%, respectively, compared to LPS-treated BMDMs from control mice (Figure S9C). Collectively, these *ex vivo* data clearly indicate that GHSR autonomously promotes pro-inflammatory M1 macrophage polarization in response to lipid and endotoxin stressors.

3.9. GHSR remodels M1-macrophage polarization by reprogramming metabolic pathways and NF-κB activation

Under metabolic stress, macrophages undergo extensive changes in metabolic activity, promoting pro-inflammatory cytokine production [70,71]. Increased glycolysis is a hallmark metabolic signature of M1-like macrophages and elevated fatty acid oxidation (FAO) is a hallmark metabolic signature of M2-like macrophages [71]. Since mitochondrial bioenergetics is known to play an important role in macrophage programming, we investigated the OCR in *Ghsr*-deficient and control BMDMs under PA treatment. Under both solvent (BSA) and PA, we observed a higher OCR in *Ghsr*-deficient BMDMs than that in control BMDMs, while the difference was more pronounced under PA (Figure 6A). The basal and maximal respiration rates were significantly increased in PA-treated *Ghsr*-deficient BMDMs, compared to that of control BMDMs, showing 93.7% and 89.3% increase, respectively (Figure 6A). Since GHSR deficiency decreases pro-inflammatory M1 macrophage polarization, we further investigated the glycolytic rate of *Ghsr*-deficient macrophages. As expected, LPS enhanced both basal and compensatory glycolysis in control BMDMs, while those of saline-treated BMDMs were comparable between genotypes. Interestingly, *Ghsr*-deficient BMDMs showed reduced compensatory glycolysis under LPS stimulation (Figure 6B). *Ghsr* deficiency reduced LPS-induced glycolysis, which is in line with the macrophage phenotype of reduced pro-inflammatory polarization.

It is known that NF-κB nuclear translocation drives macrophage pro-inflammatory polarization that is linked to metabolic pathways such as
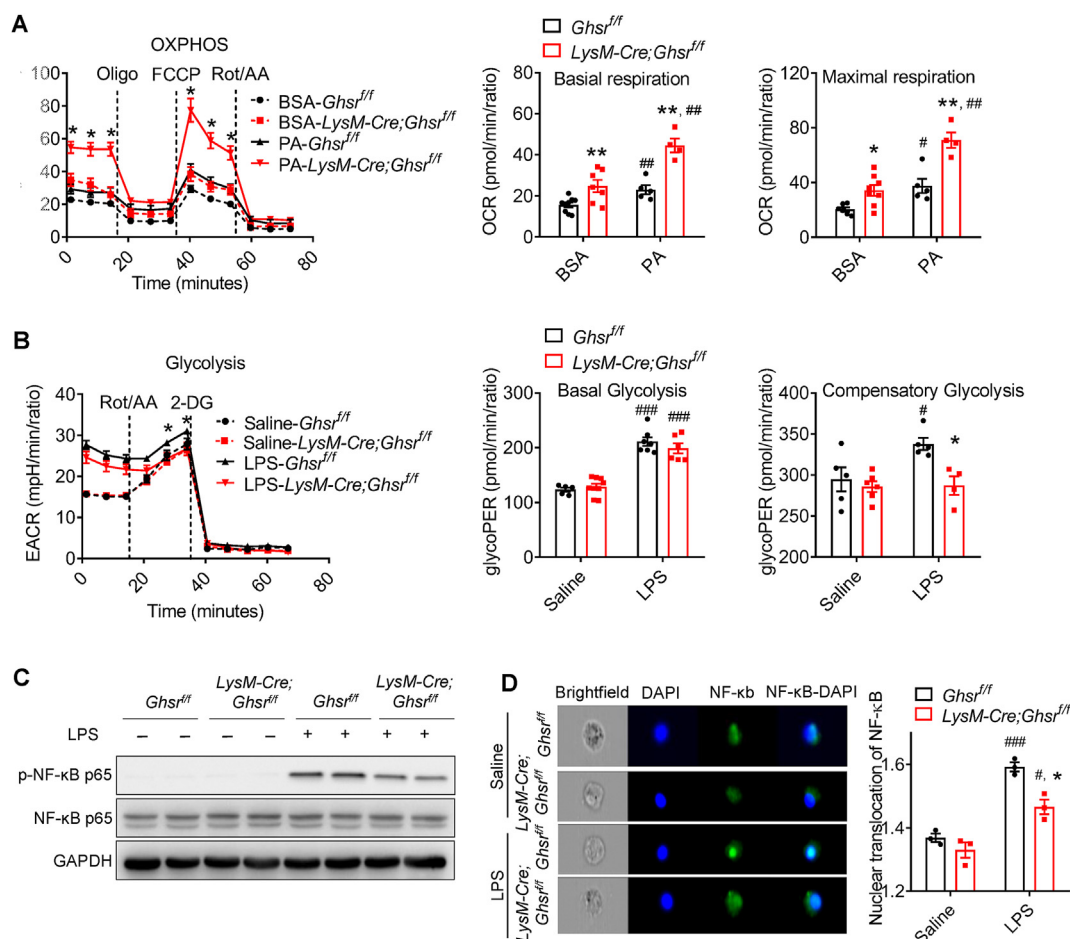

Figure 6: Myeloid-specific *Ghsr* deficiency reprograms metabolic pathways and suppresses NF-κB activation in BMDMs. (A) OXPHOS measured as OCR in PA-treated BMDMs of control and *LysM-Cre;Ghsr^f/f^*, n = 4−8/group. (B) Assessment of extracellular acidification rate (ECAR) in BMDMs using Seahorse extracellular flux analyzer, n = 4−9/group. (C) The protein levels of phosphorylated p65 in BMDMs, n = 2/group; Independent experiments were repeated two times. (D) Nuclear translocation of NF-κB p65 in BMDMs by ImageStream. The average count of macrophages in the three samples of each group of Saline-control, Saline-*Ghsr* deficient, lipopolysaccharide (LPS)-control, or LPS-*Ghsr* deficient BMDMs were 8795, 8651, 10,056, and 10,804, respectively. n = 3/group. *$p < 0.05$, **$p < 0.01$ *LysM-Cre;Ghsr^f/f^* vs. *Ghsr^f/f^*, #$p < 0.05$, ##$p < 0.01$ ###$p < 0.001$ LPS vs. Saline.

glycolysis [72—74]. To study whether the activation of NF-κB p65 is regulated by GHSR in macrophages, we measured phosphorylation of NF-κB p65 in BMDMs. In response to LPS stimulation, *Ghsr*-deficient BMDMs showed a lower induction of phosphorylated (p)-NF-κB p65 compared to control BMDMs (Figure 6C). We further examined the level of NF-κB p65 nuclear translocation in LPS-induced BMDMs by using the ImageStream imaging flow cytometer, leveraging the combination of high-resolution digital imaging and quantitative flow cytometry technology. Similarity quantitation score was assessed using IDEAS software by quantifying the merged area of NF-κB p65 and nuclear staining (DAPI) to examine the correlation of NF-κB p65/DAPI co-localization. When we quantified the differences in nuclear localization of NF-κB between saline-treated and LPS-treated BMDMs from control mice, the similarity score of NF-κB nuclear translocation was significantly higher in the LPS-treated group (Figure 6D). Remarkably, *Ghsr* deficiency significantly decreased the LPS-induced NF-κB p65 translocation to nucleus. These results suggest that the attenuated M1 macrophage polarization in LPS-treated *Ghsr*-deficient BMDMs is, at least in part, due to the reduced nuclear translocation of NF-κB.

3.10. GHSR reprograms macrophage polarization via protein kinase A (PKA) and AKT2 signaling

Previous studies have reported that insulin signaling in macrophages contributes to macrophage polarization and shifts the metabolic pathway toward glycolysis [70,75,76]. In ovarian preantral granulosa cells, it has been shown that GPCR-mediated PKA signaling stimulates phosphorylation of CREB and reduces the activity of insulin signaling [77,78]. In β cells, CREB has been shown to increase insulin receptor substrate 2 (IRS2) expression [79,80]. However, the roles of these pathways in macrophages are not clear. Interestingly, we found that while LPS treatment significantly increased p-CREB, IRS2, and p-AKT in control BMDMs, remarkably, *Ghsr*-deficient BMDMs showed significantly reduced expression of p-CREB, IRS2, and p-AKT under LPS stimulation (Figure 7A). Thus, we hypothesized that GHSR regulates macrophage polarization through PKA-CREB and insulin signaling. To test this hypothesis, we used a small interfering RNA (siRNA) approach to silence the gene expression of protein kinase cAMP-activated catalytic subunit alpha (*Prkaca*), a gene responsible for encoding catalytic subunits of PKA. In the scrambled siRNA group, LPS-treated *Ghsr*-deficient BMDMs showed significantly decreased gene expression of pro-inflammatory cytokine genes, such as *Il1b* and *Il6* by 44.7% and 25.4%, respectively, compared to that in LPS-treated control BMDMs (Figure 7B). As expected, *Prkaca* knockdown significantly reduced gene expression levels of pro-inflammatory cytokine genes, such as *Tnfa*, *Il1b*, and *Il6* by 36.5%, 60.1%, and 49.8%, respectively, in control BMDMs. *Ghsr*-deficient BMDMs did not show further suppression of pro-inflammatory genes by *Prkaca* knockdown (Figure 7B). That is to note, the suppression of pro-inflammatory cytokine gene expression in macrophage GHSR deficiency or *Prkaca* knockdown was not detected under saline condition (Figure S10A). To mimic HFD *in vitro*, we challenged the BMDMs with PA and assessed the inflammatory response of *Prkaca* knockdown. In line with the results in the LPS-treated group (Figure 7B), gene expression levels of pro-inflammatory cytokine genes, such as *Il1b* and *Il6* were significantly reduced by *Prkaca* knockdown in control BMDMs, whereas *Prkaca* knockdown did not further reduce these pro-inflammatory gene expressions in PA-treated *Ghsr*-deficient BMDMs (Figure S10B). Taken together, these results suggest that *Ghsr* deficiency suppresses macrophage pro-inflammatory activation through inhibition of PKA signaling.

3.11. *Ghsr* overexpression exacerbates pro-inflammatory responses in macrophages by enhancing PKA-regulated insulin signaling

To further validate the effect of GHSR on programming macrophage polarization, we also employed a gain-of-function approach by over-expressing *Ghsr* in murine macrophage RAW264.7 cells. As expected, *Ghsr* expression was dramatically increased in *Ghsr*-overexpressed RAW264.7 cells (Figure S11A). *Ghsr* overexpression in macrophages activated inflammatory response, evident in the elevated *Tnfa* and *Il6* expression (Figure S11B). Importantly, under LPS treatment, the gene expression of *Irs2*, rather than *Irs1*, was significantly increased in *Ghsr*-overexpressing macrophages (Figure S11C). Consistently, *Ghsr* overexpression further enhanced IRS2 and phosphorylation of CREB and AKT, especially AKT2, under LPS stimulation (Figures 7C and S11D), while IRS1 expression showed no significant difference and p-AKT1 showed a slight trend of increase without statistical significance (Figure S11D). The reduction of p-AKT2, but not p-AKT1, was also detected in LPS-treated *Ghsr*-deficient BMDMs (Figure S11E). These data together suggest that AKT2 is the primary mediator of GHSR signaling in macrophages.

To further verify the necessity of IRS2-AKT2 axis in LPS-induced pro-inflammatory activation in macrophages, we knocked down IRS2 in RAW264.7 cells with siRNA-*Irs2*. Indeed, upon inhibition of *Irs2*, IRS2-AKT2 signaling was reduced, and LPS-induced NF-κB activation was significantly suppressed, evident in increase of IκBα and decrease of NF-kB phosphorylation at S536 (Figure 7D). Collectively, our studies unequivocally demonstrated that GHSR regulates PKA-CREB-IRS2-AKT2 signaling cascade to promote macrophage pro-inflammatory activation, which is a novel immunometabolic modulatory mechanism in programming of macrophage polarization.

4. DISCUSSION

We previously reported that global *Ghsr* knockout protects against age-associated low-grade inflammation in WAT and brown adipose tissue (BAT) by shifting macrophage phenotype from M1-like to M2-like macrophages [14], but it is unknown whether the phenotype is determined by the cell-autonomous effect of GHSR in macrophages. To further investigate the direct effect of GHSR in macrophages and the underpinning mechanisms, we generated a novel mouse line of myeloid-specific *Ghsr*-deleted mice. We showed that *Ghsr* expression in macrophages is transcriptionally activated by HFD, suggesting that GHSR may be involved in the pathogenesis of meta-inflammation. The current comprehensive set of studies has utilized the novel cell-type-specific mouse model to examine the roles and mechanisms of GHSR in HFD-induced meta-inflammation. Our data demonstrated that myeloid-specific *Ghsr* deficiency mitigates diet-induced systemic inflammation and insulin resistance by suppressing inflammation in metabolic tissues, including adipose tissues and liver. Moreover, we found that *Ghsr* deficiency in macrophages suppresses M1 pro-inflammatory polarization by modulating the insulin signaling cascade. Our novel findings are supported by several lines of compelling *in vivo* and *ex vivo* evidence: First, myeloid-specific *Ghsr* deficiency reduced macrophage infiltration and pro-inflammatory polarization of macrophages in eWAT and liver tissues. Second, monocytes of myeloid-specific *Ghsr*-deleted mice expressed lower levels of chemokine receptor CCR2, supporting reduced macrophage migration into eWAT and liver tissues. Third, GHSR loss-of-function and gain-of-function results unequivocally demonstrated that GHSR is a critical regulator of macrophage polarization, and that GHSR remodels macrophage polarization by modulating the PKA-CREB-IRS2-AKT2
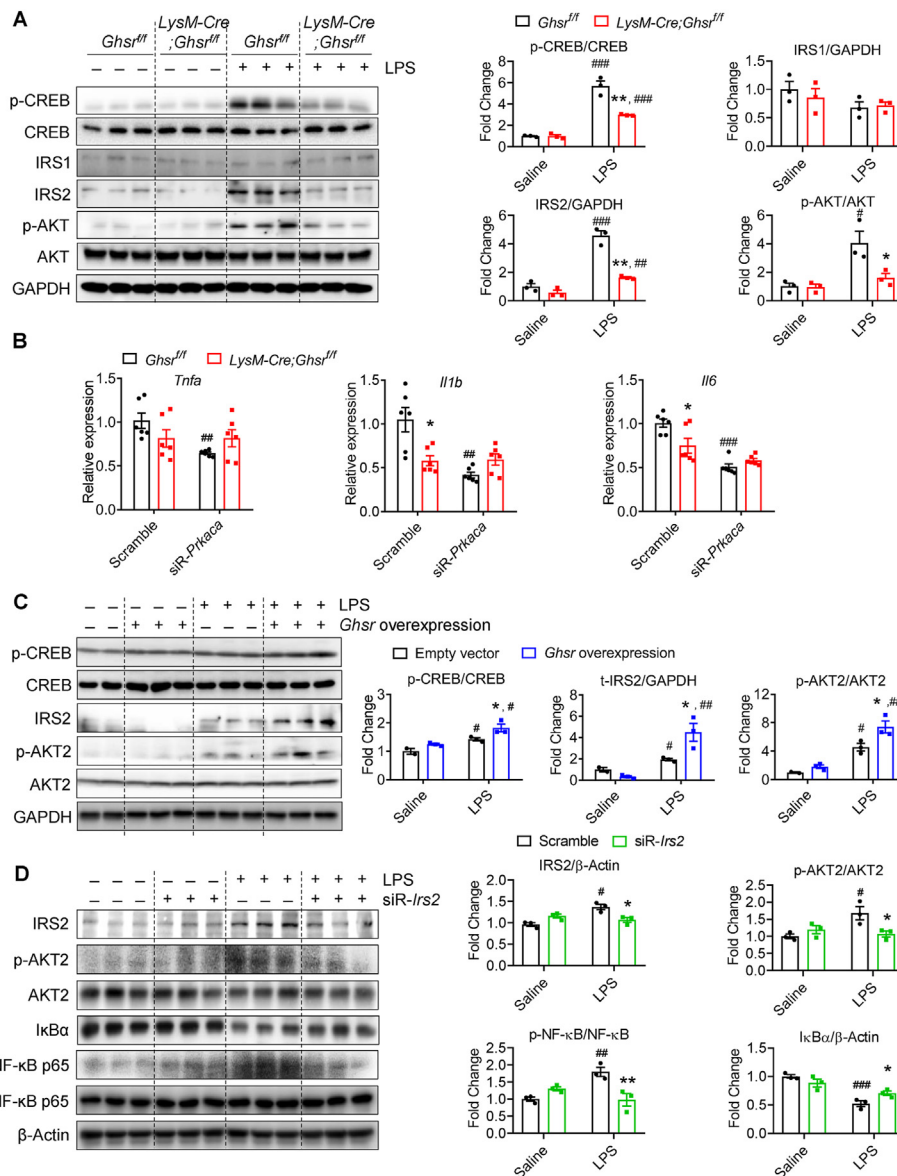
Figure 7: Macrophage GHSR regulates LPS-induced pro-inflammatory response via activation of CREB and IRS2-AKT2 in macrophages. (A) Protein levels of phosphorylated (p)/t-CREB, IRS1, IRS2, p/t-AKT signaling in LPS-stimulated BMDMs of control and *LysM-Cre;Ghsr^{f/f}* mice. Independent experiments were repeated 3 times. (B) Gene expression of pro-inflammatory cytokines in LPS-stimulated BMDMs of control and *LysM-Cre;Ghsr^{f/f}* mice transfected with siR-*Prkaca* or control siRNA (scramble), n = 4−6/group. (C) Protein levels of p/t-CREB and insulin signaling of IRS2 and p/t-AKT2 in LPS-treated RAW264.7 cells transfected with pcDNA3.1-Ghsr or empty vector, n = 2−3/group. (D) Protein levels of IRS2, p/t-AKT2, p/t-NF-κB p65, and IκBα in LPS-treated RAW264.7 cells transfected with siR-*Irs2* or control scramble, n = 3/group. Data are presented as the means ± SEM. *$P < 0.05$, **$P < 0.01$, ***$P < 0.001$ by two-way ANOVA (B−D), *LysM-Cre;Ghsr^{f/f}* vs *Ghsr^{f/f}*, *Ghsr* overexpression vs. empty vector, or siR-*Irs2* vs. scramble, #$P < 0.05$, ##$P < 0.01$, ###$P < 0.001$ by two-way ANOVA (B−D), LPS vs. Saline or siR-*Prkaca* vs. Scramble. n represents the number of technical replicates.

signaling cascade. These novel results demonstrate that myeloid-specific *Ghsr* deficiency attenuates chronic inflammation and improves diet-induced metabolic dysfunction, suggesting that macrophage GHSR could be a potential therapeutic target for meta-inflammation.

Our study is the first report to elucidate the cell-autonomous effect of GHSR on macrophage programming under diet-induced meta-inflammation. In this study, we have assessed the myeloid-specific *Ghsr*-deficient mice under both homeostatic RD feeding and an overnutrition state of HFD feeding. RD-fed *LysM-Cre;Ghsr^{f/f}* mice showed comparable body weight, fat mass, and metabolic characteristics, which indicate that myeloid-specific GHSR does not play a

major role in lean mice under homeostatic condition. Interestingly, we found that HFD feeding significantly increased *Ghsr* gene expression in PMs, suggesting that GHSR plays an important role in HFD-induced meta-inflammation. Under HFD feeding, *LysM-Cre;Ghsr^{f/f}* mice did not show changes in body weight, fat mass, nor metabolic profile; but showed significant improvements in inflammation, glucose intolerance, and systemic insulin sensitivity. Specifically, our study showed that myeloid-specific *Ghsr* ablation attenuated HFD-induced systemic and tissue inflammation in adipose tissue and liver. These results suggest that GHSR functions as an important nutrient sensor in macrophages modulating diet-induced chronic inflammation and metabolic dysregulation. Although body weight and fat mass are often

correlated with insulin sensitivity, it has also been reported that body weight and fat mass are not always coupled with insulin sensitivity [81,82]. In our previous study, we found that global *Ghsr* ablation does not affect body weight under HFD feeding [83], but alleviates adipose tissue inflammation and insulin resistance in aging [14]. We also observed that global *Ghsr* ablation attenuates high fructose corn syrup (HFCS)-induced adipose inflammation and insulin resistance without altering body weight or fat composition [26]. These results indicate that macrophage GHSR has differential effects on inflammation and metabolism; GHSR in macrophages serves as an "immune sensor" responsive to lipid toxicity and endotoxin, playing an important pathogenic role in meta-inflammation and insulin resistance.

In our study, we also found that serum pro-inflammatory cytokine levels were significantly reduced in myeloid-specific *Ghsr*-deficient mice under HFD feeding, suggesting that myeloid-specific *Ghsr* deficiency mitigates HFD-induced systemic inflammation. More importantly, our results showed that myeloid-specific *Ghsr* deficiency reduced expression of CCR2 in the Ly6Chi monocyte subset of PBMCs. The Ly6Chi monocyte subset has been linked to promoting influx of monocytes into inflamed tissues [49,50]; this is exciting that myeloid-specific *Ghsr* deficiency attenuates systemic and local inflammation through downregulation of CCR2 in monocytes. This new finding suggests that GHSR in monocytes remodels monocyte mobilization, recruitment, and tissue infiltration. GHSR in myeloid cell lineage may have a prominent role in the pathogenesis of meta-inflammation and further investigation in this area is likely to be fruitful.

It is known that eWAT is a primary contributor to insulin resistance under DIO, and obesity-induced macrophage infiltration is higher in eWAT than in liver and skeletal muscle [75]. As expected, our results showed that IM population was significantly increased in eWAT of HFD-fed control mice. Remarkably, myeloid-specific *Ghsr* deficiency significantly decreased IM population in eWAT under HFD feeding. CX3CR1 has been used a marker for monocyte-derived macrophages to distinguish between infiltrating and resident macrophages [51]. We found that the percentage of CX3CR1-positive cells was significantly lowered in IM populations in eWAT of HFD-fed *LysM-Cre;Ghsr^{f/f}* mice than in that of controls. These results indicate that myeloid-specific *Ghsr* deficiency alleviates HFD-induced macrophage infiltration and decreases pro-inflammation in eWAT, which is consistent with the improved insulin sensitivity exhibited by HFD-fed *LysM-Cre;Ghsr^{f/f}* mice. Moreover, we observed that myeloid-specific *Ghsr* deficiency increased serum adiponectin levels. Previous studies showed that inguinal fat (iWAT) expansion increases adiponectin and enhances insulin sensitivity [84]. However, we found that myeloid-specific *Ghsr* deficiency had no effect on iWAT/body weight percentage, inflammatory gene expression, and percentage of IM subset (data not shown) in iWAT. Therefore, increased serum adiponectin in myeloid-specific *Ghsr*-deficient mice is most likely attributed to the improved metabolic function of eWAT. These results collectively suggest that eWAT, but not iWAT, is the key tissue that contributes to the improved insulin sensitivity of HFD-fed *LysM-Cre;Ghsr^{f/f}* mice.

The liver is another important metabolic organ that controls body energy metabolism and insulin sensitivity [85]. We found that HFD feeding significantly increased liver IM population without affecting KC population. Furthermore, myeloid-specific *Ghsr* deficiency significantly decreased IM population and CX3CR1+ IM subset in liver under HFD feeding. The results indicate that myeloid-specific *Ghsr* deficiency attenuates liver macrophage infiltration and decreases liver inflammation. Consistent with our current results, several studies reported that over-nutritional status increases macrophage infiltration in the liver [51,86,87]. A recent publication also reported that Tim4-associated resident KCs are depleted under HFD feeding [55]. Although KCs have been widely defined as F4/80highCD11bint/+ in flow cytometry, Tim4 and Clec4F are now utilized as specific markers to distinguish subtypes of KCs. In contrast to F4/80, Tim4 and Clec4F are detectable in mature KCs but are absent in IMs or monocyte-derived KCs (mo-KCs) [55,88]. This might be a possible explanation for the discrepant patterns between Tim4+ and Clec4F+ KCs and F4/80high KCs under HFD feeding [55,89]. We acknowledge the caveat of our gating strategy using F4/80high as a KC marker which likely detects all KCs, including mo-KCs. In addition, we found that myeloid-specific *Ghsr* deficiency decreased liver lipid accumulation. In eWAT, lipolysis-related gene expression was decreased, and serum FFA was consistently reduced in HFD-fed myeloid-specific *Ghsr*-deficient mice. Thus, it is possible that, in HFD-fed myeloid-specific *Ghsr*-deficient mice, decreased eWAT-associated FFA influx to the liver contributes to reduced liver lipid deposition. Liver FAO-related genes were significantly upregulated in myeloid-specific *Ghsr*-deficient mice, which may also contribute to decreased lipid deposition in liver. Our result of primary hepatocytes cultured with BMDM-CM further showed that secretum from *Ghsr*-deficient BMDMs enhanced gene expression of *Ppara* and *Cpt1* and Seahorse functional assessment of β-oxidation in PA-treated primary hepatocytes, suggesting that secretory factors from *Ghsr*-deficient BMDMs directly affect FAO in primary hepatocytes. The detailed mechanisms of the macrophage and hepatocyte crosstalk warrant further investigation.

Myeloid cells include not only macrophages, but also monocytes and neutrophils. LysM promoter can induce Cre activity in all myeloid cells, so the *in vivo* phenotype we observed may not be solely due to macrophages. Thus, in addition to macrophages, we also examined other types of myeloid cells such as monocytes and neutrophils. In PBMC, we found expression of CCR2 in the Ly6Chi monocyte subset is significantly reduced in HFD-fed myeloid-specific *Ghsr*-deficient mice. Our data showed that diet-induced increase of myeloid cells in eWAT and liver was primarily due to increased macrophages, not neutrophils. In eWAT and liver, myeloid-specific *Ghsr* deficiency under HFD feeding decreased the percentage of myeloid cells and macrophage subsets, but no difference was observed in neutrophils. Decreased macrophage infiltration associated with myeloid-specific *Ghsr* deficiency may further lead to reduced macrophage-mediated adipose and hepatic inflammation in DIO. Neutrophils with short life span transiently infiltrate into adipose tissue early in the course of HFD feeding [90,91]. Indeed, the insulin resistance of long-term HFD exposure has been mostly associated with macrophage-mediated pro-inflammation [92]. In our DIO mouse model, we treated mice with HFD for 5 months. The improvement we observed in chronic inflammation and insulin resistance in myeloid-specific *Ghsr*-deficient mice is most likely attributed to *Ghsr* deficiency in macrophages, not neutrophils.

It is known that M1-like pro-inflammatory macrophages is commonly associated with insulin resistance under DIO [93,94]. Indeed, our data showed that *Ghsr*-deficient PMs under HFD-feeding exhibited decreased M1-like macrophage polarization and reduced intracellular pro-inflammatory cytokines in the macrophages. Consistently, *Ghsr* deficiency decreased PA- or LPS-induced M1-like macrophage polarization, showing changes in cell surface marker expression and pro-inflammatory cytokines in BMDMs. Macrophage activation and lipid metabolism are closely linked to the metabolic reprogramming of M1-like and M2-like macrophages [95,96]. While increased glycolysis is a metabolic signature of M1-like macrophages, increased FAO is a metabolic signature of M2-like macrophages [71]. Consistent with phenotypic observation, our Seahorse data revealed that *Ghsr* deficiency in macrophages enhanced FAO and reduced glycolysis, which supports that GHSR promotes M1 macrophage polarization. The pro-

inflammatory nuclear transcription factor, NF-κB, is a major regulator of macrophage energy metabolism promoting glycolysis [97]. Consistently, we detected reduced nuclear translocation and phosphorylation of NF-κB in LPS-treated *Ghsr*-deficient BMDMs. Therefore, GHSR likely remodels macrophage energy metabolism through regulating the activity of NF-κB.

Under the inflammation stressor of LPS, we found that *Ghsr* deficiency induced anti-inflammation in macrophages via inhibition of PKA. Under LPS treatment, *Ghsr*-deficient BMDMs exhibited downregulation of p-CREB, while *Ghsr*-overexpressed RAW264.7 cells exhibited upregulation of p-CREB. Previous studies show that the PKA-CREB pathway is involved in macrophage polarization [98,99]. Our results indicate that GHSR in macrophages modulates M1-like macrophage polarization, through PKA-CREB signaling. Insulin signaling is a master regulatory pathway of metabolism. Insulin receptor deficiency in macrophages protects against inflammation [75,100,101], and insulin signaling is involved in macrophage polarization [102]. IRS2 is a major insulin mediator in macrophages [103], and IRS2 deletion promotes IL4-induced M2 macrophage polarization [104]. Our results are in support of the activation of insulin signaling in macrophages promotes pro-inflammatory macrophage polarization. Intriguingly in our LPS-treated BMDMs, *Irs2* gene expression was decreased when the activity of CREB was inhibited by *Prkaca* siRNA, and *Ghsr* deficiency down-regulated protein levels of IRS2 and p-AKT, but had no significant effect on IRS1. Consistently, under LPS-induced inflammation, overexpression of *Ghsr* in RAW264.7 cells increased IRS2, but not IRS1. These results suggest that GHSR promotes M1-like macrophage polarization through transcriptional activation of IRS2. Interestingly, our current study showed that the effect of GHSR on IRS2 expression in macrophages was more pronounced under the LPS-induced pro-inflammatory state. *Ghsr* overexpression only enhanced IRS2 expression under LPS, not under saline. Our data support that the activation of the GHSR-IRS2 axis takes place under inflammatory condition, and GHSR-insulin signaling plays an important role in macrophage M1 pro-inflammatory polarization.

We further showed that overexpressing *Ghsr* in macrophages enhanced LPS-stimulated p-AKT2. While *Ghsr* overexpression slightly increased phosphorylation of AKT1 (not statistically significant) in RAW264.7 cells, *Ghsr* deficiency in BMDMs significantly reduced the phosphorylation of AKT2, not AKT1, suggesting that GHSR in macrophages primarily affects AKT2 phosphorylation. *Irs2*-knockdown macrophages had lower LPS-induced phosphorylation of AKT2 and NF-κB p65 compared to that of control macrophages, solidifying the role of IRS2-AKT2 in M1 macrophage polarization. Several studies have reported the differential sensitivity of AKT isoforms to IRS1 or IRS2. In L6 myotubes, Huang et al. found that loss of IRS2 results in a reduction of AKT2 phosphorylation, while IRS1 is responsible for both AKT1 and AKT2 phosphorylation [105]. In insulin-secreting cells, silencing of c-Jun N-terminal Kinase 3 (JNK3) strongly downregulates IRS2 and p-AKT2 expression but not p-AKT1 under insulin treatment, while the silencing of JNK1 or JNK2 activates both AKT1 and AKT2 [106]. While it is unknown whether IRS1 and IRS2 mediate distinct AKT isoforms in macrophages, it is widely accepted that the AKT signaling pathway has a direct effect on macrophage polarization [107]. In the recent report, AKT isoforms differentially contribute to macrophage polarization: AKT1 and AKT2 ablation results in M1 and M2 phenotype, respectively [76]. PBMCs and PMs of AKT2-null mice exhibit reduced HFD-induced CCR2-expressing Ly6Chi monocyte percentages and LPS-induced inflammation, indicating a suppressed M1-like macrophage polarization [108]. In our myeloid-specific *Ghsr*-deficient mice, we found downregulated CCR2 expression in the Ly6Chi monocyte subset, and reduced inflammation in

macrophages. Therefore, the mechanisms of GHSR-mediated M1 polarization likely is through the PKA-CREB-IRS2-AKT2 signaling cascade. In addition to the change in macrophage infiltration and M1/M2 polarization, LAMs have emerged as an important class of macrophages in obesity. LAMs are increased under obese condition, and regulates lipid uptake and metabolism to protect against adipose tissue and liver dysfunction [53,56]. In the current study, we found that expression of LAM-related genes, especially *Trem2*, was significantly upregulated in eWAT, liver, and PMs of myeloid-specific *Ghsr* deficiency mice under HFD feeding. Recent studies revealed that *Trem2* deficiency in macrophages causes impaired lipid handling, cell death, and fibrosis, indicating TREM2 signaling is essential for LAMs to prevent systemic metabolic dysregulation and progression of NAFLD [54,109]. Therefore, the beneficial effect of *Ghsr*-deficient macrophages may be, at least in part, mediated by the regulation of LAMs. Investigation of the interrelation between GHSR and TREM2 pathway in LAMs is warranted. Several studies reveal that over-nutritional status, such as obesity, is accompanied by decreased serum ghrelin levels [110—112]. Indeed, our current study shows that active ghrelin levels in the serum of HFD-fed control mice were lower than those of RD-fed mice (no significance). Interestingly, our current study demonstrated that gene expression of *Ghsr* in PMs is significantly increased under HFD feeding. It is possible that the elevated GHSR in macrophages is a compensatory response to the reduced ghrelin levels under obesity. A previous study in the heart of human patients shows that impaired ghrelin production during chronic heart failure resulted in increased GHSR expression in myocardium [113]. A study in rats shows that plasma ghrelin levels significantly decreased during sepsis, while GHSR expression in aorta, heart, and small intestine is markedly elevated in early sepsis [114]. These studies suggest the compensatory effect of reduced ghrelin levels on increased GHSR expression. However, the direct feedback regulation between ghrelin and GHSR remains to be validated. Whether any other factors participate in the upregulation of *Ghsr* expression in PMs of HFD-fed mice needs to be further investigated.

The effects of ghrelin on inflammation are controversial; both pro-inflammatory and anti-inflammatory effects have been reported [115—117]. Ghrelin shows protective effects during the early phase of sepsis but impairs immune responses during the latter phase, and its adverse effects are more detrimental in lean mice than obese mice [118]. Recent reports suggest that acyl- and desacyl-ghrelin have effects on macrophage polarization under inflammatory condition *in vitro*; suppression of M1-like pro-inflammatory macrophage polarization is observed in ghrelin-treated RAW264.7 cells [119,120]. In contrast, short-term acyl-ghrelin treatment enhances the effect of LPS to increase pro-inflammatory macrophage polarization [121]. In addition, it has been suggested that ghrelin has both GHSR dependent and independent effects: ghrelin induces the release of growth hormone and food intake via GHSR [20,122], but stimulates osteoblast growth and liver glucose production by mechanisms independent of GHSR [123—125].

Moreover, GHSR is a G protein-coupled receptor, which is known to have high constitutive activity and GHSR signaling can be activated in the absence of ghrelin [126]. In our current study, *Ghsr* overexpression in RAW264.7 cells promoted pro-inflammation as indicated by significantly increased gene expression of *Tnfa* and *Il6* and protein expression levels of p-CREB, IRS2, and p-AKT2. We previously reported that ghrelin null mice and GHSR null mice have different thermogenic phenotypes and susceptibility to diet-induced adipose inflammation [26,123,127]. High constitutive activity of GHSR also

Original Article

affects downstream signaling and physiological processes in the ligand-independent manner [128,129]. Thus, the investigation is much needed to determine the controversial actions of ghrelin on macrophages and the constitutive activity of GHSR under physiological and pathological conditions.

In conclusion, our findings demonstrate for the first time that nutrient-sensing GHSR is a novel immunoregulator of macrophages, which has a critical role in macrophage remodeling under obesity. Myeloid-specific *Ghsr* deficiency attenuates diet-induced meta-inflammation and improves systemic insulin sensitivity. Specifically: 1) In circulation, myeloid-specific *Ghsr* deficiency decreases serum pro-inflammatory cytokines and reduces *Ghsr* expression in pro-inflammatory Ly6C^{hi} monocytes. 2) In the eWAT and liver, myeloid-specific *Ghsr* deficiency decreases macrophage infiltration and M1-like macrophage polarization, exhibiting reduced tissue inflammation. 3) Mechanistically, GHSR reprograms macrophage polarization through the PKA-CREB-IRS2-AKT2 signaling cascade. Our novel observations in this study reveal that nutrient-sensing GHSR in macrophages is responsive to HFD-induced lipid toxicity and functions as a critical immune sensor, leading to the remodeling of macrophages. Our findings indicate that suppressing GHSR signaling in macrophages may serve as a novel immuno-therapeutic strategy for controlling meta-inflammation in obesity-related inflammatory diseases/conditions.

CONTRIBUTION

DK performed experiments, analyzed data, and wrote the manuscript. JHL generated mouse model, performed experiments, and wrote the manuscript. PQ, HH, ZS, SE, CW, WY, and JN performed experiments, analyzed data, and edited the manuscript. DWT, SG, GW, and RA helped to troubleshoot the study and edited the manuscript. YS conceived the study, revised the manuscript, and provided funding. All authors contributed to and approved the final version of the manuscript.

ACKNOWLEDGMENT

DECLARATION OF COMPETING INTEREST

The authors declare that they have no known competing financial interests or personal relationships that could have appeared to influence the work reported in this paper.

DATA AVAILABILITY

Data will be made available on request.

APPENDIX A. SUPPLEMENTARY DATA

Supplementary data to this article can be found online at https://doi.org/10.1016/j.molmet.2023.101852.

REFERENCES

[1] Uysal KT, Wiesbrock SM, Marino MW, Hotamisligil GS. Protection from obesity-induced insulin resistance in mice lacking TNF-alpha function. Nature 1997;389(6651):610—4.

[2] Xu H, Barnes GT, Yang Q, Tan G, Yang D, Chou CJ, et al. Chronic inflammation in fat plays a crucial role in the development of obesity-related insulin resistance. J Clin Investig 2003;112(12):1821—30.

[3] McGarry JD. Banting lecture 2001: dysregulation of fatty acid metabolism in the etiology of type 2 diabetes. Diabetes 2002;51(1):7—18.

[4] Sachithanandan N, Graham KL, Galic S, Honeyman JE, Fynch SL, Hewitt KA, et al. Macrophage deletion of SOCS1 increases sensitivity to LPS and palmitic acid and results in systemic inflammation and hepatic insulin resistance. Diabetes 2011;60(8):2023—31.

[5] Czaja AJ, Manns MP. Advances in the diagnosis, pathogenesis, and management of autoimmune hepatitis. Gastroenterology 2010;139(1):58—72 e54.

[6] Weber A, Boege Y, Reisinger F, Heikenwalder M. Chronic liver inflammation and hepatocellular carcinoma: persistence matters. Swiss Med Wkly 2011;141:w13197.

[7] Bhargava P, Lee CH. Role and function of macrophages in the metabolic syndrome. Biochem J 2012;442(2):253—62.

[8] Wynn TA, Barron L. Macrophages: master regulators of inflammation and fibrosis. Semin Liver Dis 2010;30(3):245—57.

[9] Li C, Xu MM, Wang K, Adler AJ, Vella AT, Zhou B. Macrophage polarization and meta-inflammation. Transl Res J Lab Clin Med 2018;191:29—44.

[10] Hertzel AV, Yong J, Chen X, Bernlohr DA. Immune modulation of adipocyte mitochondrial metabolism. Endocrinology 2022;163(8).

[11] Jenkins SJ, Ruckerl D, Thomas GD, Hewitson JP, Duncan S, Brombacher F, et al. IL-4 directly signals tissue-resident macrophages to proliferate beyond homeostatic levels controlled by CSF-1. J Exp Med 2013;210(11):2477—91.

[12] Jenkins SJ, Ruckerl D, Cook PC, Jones LH, Finkelman FD, van Rooijen N, et al. Local macrophage proliferation, rather than recruitment from the blood, is a signature of TH2 inflammation. Science 2011;332(6035):1284—8.

[13] Chawla A, Nguyen KD, Goh YP. Macrophage-mediated inflammation in metabolic disease. Nat Rev Immunol 2011;11(11):738—49.

[14] Lin L, Lee JH, Buras ED, Yu K, Wang R, Smith CW, et al. Ghrelin receptor regulates adipose tissue inflammation in aging. Aging 2016;8(1):178—91.

[15] Adelman K, Kennedy MA, Nechaev S, Gilchrist DA, Muse GW, Chinenov Y, et al. Immediate mediators of the inflammatory response are poised for gene activation through RNA polymerase II stalling. Proc Natl Acad Sci U S A 2009;106(43):18207—12.

[16] Miao H, Ou J, Ma Y, Guo F, Yang Z, Wiggins M, et al. Macrophage CGI-58 deficiency activates ROS-inflammasome pathway to promote insulin resistance in mice. Cell Rep 2014;7(1):223—35.

[17] Wang X, Cao Q, Yu L, Shi H, Xue B, Shi H. Epigenetic regulation of macrophage polarization and inflammation by DNA methylation in obesity. JCI Insight 2016;1(19):e87748.

[18] Tschop M, Lahner H, Feldmeier H, Grasberger H, Morrison KM, Janssen OE, et al. Effects of growth hormone replacement therapy on levels of cortisol and cortisol-binding globulin in hypopituitary adults. Eur J Endocrinol 2000;143(6):769—73.

[19] Kojima M, Kangawa K. Ghrelin: structure and function. Physiol Rev 2005;85(2):495—522.

[20] Sun Y, Wang P, Zheng H, Smith RG. Ghrelin stimulation of growth hormone release and appetite is mediated through the growth hormone secretagogue receptor. Proc Natl Acad Sci U S A 2004;101(13):4679—84.

[21] Lin L, Saha PK, Ma X, Henshaw IO, Shao L, Chang BH, et al. Ablation of ghrelin receptor reduces adiposity and improves insulin sensitivity during aging by regulating fat metabolism in white and brown adipose tissues. Aging Cell 2011;10(6):996—1010.

[22] Lin L, Nuotio-Antar AM, Ma X, Liu F, Fiorotto ML, Sun Y. Ghrelin receptor regulates appetite and satiety during aging in mice by regulating meal Frequency and portion size but not total food intake. J Nutr 2014;144(9):1349—55.

[23] Zigman JM, Jones JE, Lee CE, Saper CB, Elmquist JK. Expression of ghrelin receptor mRNA in the rat and the mouse brain. J Comp Neurol 2006;494(3): 528—48.

[24] Lee JH, Lin L, Xu P, Saito K, Wei Q, Meadows AG, et al. Neuronal deletion of ghrelin receptor almost completely prevents diet-induced obesity. Diabetes 2016;65(8):2169—78.

[25] Dixit VD, Schaffer EM, Pyle RS, Collins GD, Sakthivel SK, Palaniappan R, et al. Ghrelin inhibits leptin-and activation-induced proinflammatory cytokine expression by human monocytes and T cells. J Clin Investig 2004;114(1): 57—66.

[26] Ma X, Lin L, Yue J, Pradhan G, Qin G, Minze LJ, et al. Ghrelin receptor regulates HFCS-induced adipose inflammation and insulin resistance. Nutr Diabetes 2013;3:e99.

[27] Clausen BE, Burkhardt C, Reith W, Renkawitz R, Forster I. Conditional gene targeting in macrophages and granulocytes using LysMcre mice. Transgenic Res 1999;8(4):265—77.

[28] Lian Z, Perrard XD, Peng X, Raya JL, Hernandez AA, Johnson CG, et al. Replacing saturated fat with unsaturated fat in western diet reduces foamy monocytes and atherosclerosis in male Ldlr(-/-) mice. Arterioscler Thromb Vasc Biol 2020;40(1):72—85.

[29] Wu H, Ghosh S, Perrard XD, Feng L, Garcia GE, Perrard JL, et al. T-cell accumulation and regulated on activation, normal T cell expressed and secreted upregulation in adipose tissue in obesity. Circulation 2007;115(8): 1029.

[30] Brake DK, Smith EOB, Mersmann H, Smith CW, Robker RL. ICAM-1 expression in adipose tissue: effects of diet-induced obesity in mice. Am J Physiol Cell Physiol 2006;291(6):C1232—9.

[31] Holt MP, Cheng L, Ju C. Identification and characterization of infiltrating macrophages in acetaminophen-induced liver injury. J Leukoc Biol 2008;84(6):1410—21.

[32] Zhang X, Goncalves R, Mosser DM. The isolation and characterization of murine macrophages. Curr Protoc Immunol 2008;83(1):14.11. 11—14.11. 14.

[33] Weischenfeldt J, Porse B. Bone marrow-derived macrophages (BMM): isolation and applications. Cold Spring Harb Protoc 2008. 2008(12): pdb.prot5080.

[34] Li Q, Lei F, Tang Y, Pan JS, Tong Q, Sun Y, et al. Megalin mediates plasma membrane to mitochondria cross-talk and regulates mitochondrial metabolism. Cell Mol Life Sci 2018;75(21):4021—40.

[35] Eshghjoo S, Kim DM, Jayaraman A, Sun Y, Alaniz RC. A comprehensive high-efficiency protocol for isolation, culture, polarization, and glycolytic characterization of bone marrow-derived macrophages. J Vis Exp 2021;168.

[36] Trask Jr OJ. Nuclear factor kappa B (NF-κB) translocation assay development and validation for high content screening. Assay guidance manual. 2012 [Internet].

[37] Jiang H, Betancourt L, Smith RG. Ghrelin amplifies dopamine signaling by cross talk involving formation of growth hormone secretagogue receptor/dopamine receptor subtype 1 heterodimers. Mol Endocrinol 2006;20(8): 1772—85.

[38] Chomczynski P, Sacchi N. Single-step method of RNA isolation by acid guanidinium thiocyanate-phenol-chloroform extraction. Anal Biochem 1987;162(1):156—9.

[39] Meadows A, Lee JH, Wu CS, Wei Q, Pradhan G, Yafi M, et al. Deletion of G-protein-coupled receptor 55 promotes obesity by reducing physical activity. Int J Obes 2016;40(3):417—24.

[40] Sun Y, Garcia JM, Smith RG. Ghrelin and growth hormone secretagogue receptor expression in mice during aging. Endocrinology 2007;148(3):1323—9.

[41] Verhulst PJ, De Smet B, Saels I, Thijs T, Ver Donck L, Moechars D, et al. Role of ghrelin in the relationship between hyperphagia and accelerated gastric emptying in diabetic mice. Gastroenterology 2008;135(4):1267—76.

[42] Shoelson SE, Lee J, Goldfine AB. Inflammation and insulin resistance. J Clin Investig 2006;116(7):1793—801.

[43] Qatanani M, Lazar MA. Mechanisms of obesity-associated insulin resistance: many choices on the menu. Genes Dev 2007;21(12):1443—55.

[44] Kurihara T, Warr G, Loy J, Bravo R. Defects in macrophage recruitment and host defense in mice lacking the CCR2 chemokine receptor. J Exp Med 1997;186(10):1757—62.

[45] Palframan RT, Jung S, Cheng G, Weninger W, Luo Y, Dorf M, et al. Inflammatory chemokine transport and presentation in hev a remote control mechanism for monocyte recruitment to lymph nodes in inflamed tissues. J Exp Med 2001;194(9):1361—74.

[46] Russo L, Lumeng CN. Properties and functions of adipose tissue macrophages in obesity. Immunology 2018;155(4):407—17.

[47] Sima C, Montero E, Nguyen D, Freire M, Norris P, Serhan CN, et al. ERV1 overexpression in myeloid cells protects against high fat diet induced obesity and glucose intolerance. Sci Rep 2017;7(1):12848.

[48] Mildner A, Schönheit J, Giladi A, David E, Lara-Astiaso D, Lorenzo-Vivas E, et al. Genomic characterization of murine monocytes reveals C/EBPβ transcription factor dependence of Ly6C− cells. Immunity 2017;46(5):849—862.e847.

[49] Yang J, Zhang L, Yu C, Yang X-F, Wang H. Monocyte and macrophage differentiation: circulation inflammatory monocyte as biomarker for inflammatory diseases. Biomark Res 2014;2(1):1.

[50] Kimball A, Schaller M, Joshi A, Davis FM, denDekker A, Boniakowski A, et al. Ly6CHi blood monocyte/macrophage drive chronic inflammation and impair wound healing in diabetes mellitus. Arterioscler Thromb Vasc Biol 2018;38(5):1102—14.

[51] Serbulea V, Upchurch CM, Schappe MS, Voigt P, DeWeese DE, Desai BN, et al. Macrophage phenotype and bioenergetics are controlled by oxidized phospholipids identified in lean and obese adipose tissue. Proc Natl Acad Sci U S A 2018;115(27):E6254—63.

[52] Daemen S, Schilling JD. The interplay between tissue niche and macrophage cellular metabolism in obesity. Front Immunol 2019;10:3133.

[53] Stansbury CM, Dotson GA, Pugh H, Rehemtulla A, Rajapakse I, Muir LA. A lipid-associated macrophage lineage rewires the spatial landscape of adipose tissue in early obesity. JCI Insight 2023;8(19).

[54] Jaitin DA, Adlung L, Thaiss CA, Weiner A, Li B, Descamps H, et al. Lipid-associated macrophages control metabolic homeostasis in a Trem2-dependent manner. Cell 2019;178(3):686—698.e614.

[55] Daemen S, Gainullina A, Kalugotla G, He L, Chan MM, Beals JW, et al. Dynamic shifts in the composition of resident and recruited macrophages influence tissue remodeling in NASH. Cell Rep 2021;34(2):108626.

[56] Guilliams M, Bonnardel J, Haest B, Vanderborght B, Wagner C, Remmerie A, et al. Spatial proteogenomics reveals distinct and evolutionarily conserved hepatic macrophage niches. Cell 2022;185(2):379—396.e338.

[57] Arita Y, Kihara S, Ouchi N, Takahashi M, Maeda K, Miyagawa J-i, et al. Paradoxical decrease of an adipose-specific protein, adiponectin, in obesity. Biochem Biophys Res Commun 1999;257(1):79—83.

[58] Faraj M, Havel PJ, Phélis S, Blank D, Sniderman AD, Cianflone K. Plasma acylation-stimulating protein, adiponectin, leptin, and ghrelin before and after weight loss induced by gastric bypass surgery in morbidly obese subjects. J Clin Endocrinol Metab 2003;88(4):1594—602.

[59] Monteiro R, Azevedo I. Chronic inflammation in obesity and the metabolic syndrome. Mediat Inflamm 2010;2010:289645.

[60] Reaven GM, Hollenbeck C, Jeng C-Y, Wu MS, Chen Y-DI. Measurement of plasma glucose, free fatty acid, lactate, and insulin for 24 h in patients with NIDDM. Diabetes 1988;37(8):1020—4.

[61] Boden G. Free fatty acids as target for therapy. Curr Opin Endocrinol Diabetes Obes 2004;11(5):258—63.

[62] Boden G, She P, Mozzoli M, Cheung P, Gumireddy K, Reddy P, et al. Free fatty acids produce insulin resistance and activate the proinflammatory nuclear factor-κB pathway in rat liver. Diabetes 2005;54(12):3458–65.

[63] Karlmark KR, Weiskirchen R, Zimmermann HW, Gassler N, Ginhoux F, Weber C, et al. Hepatic recruitment of the inflammatory Gr1+ monocyte subset upon liver injury promotes hepatic fibrosis. Hepatology 2009;50(1): 261–74.

[64] Xiong X, Kuang H, Ansari S, Liu T, Gong J, Wang S, et al. Landscape of intercellular crosstalk in healthy and NASH liver revealed by single-cell secretome gene analysis. Molecular cell 2019;75(3):644–660.e645.

[65] Wang M, You Q, Lor K, Chen F, Gao B, Ju C. Chronic alcohol ingestion modulates hepatic macrophage populations and functions in mice. J Leukoc Biol 2014;96(4):657–65.

[66] Yang W, Kim DM, Jiang W, Ai W, Pan Q, Rahman S, et al. Suppression of FOXO1 attenuates inflamm-aging and improves liver function during aging. Aging Cell 2023:e13968.

[67] Yona S, Kim KW, Wolf Y, Mildner A, Varol D, Breker M, et al. Fate mapping reveals origins and dynamics of monocytes and tissue macrophages under homeostasis. Immunity 2013;38(1):79–91.

[68] Jablonski KA, Amici SA, Webb LM, Ruiz-Rosado Jde D, Popovich PG, Partida-Sanchez S, et al. Novel markers to delineate murine M1 and M2 macrophages. PLoS One 2015;10(12):e0145342.

[69] Nawaz A, Aminuddin A, Kado T, Takikawa A, Yamamoto S, Tsuneyama K, et al. CD206(+) M2-like macrophages regulate systemic glucose metabolism by inhibiting proliferation of adipocyte progenitors. Nat Commun 2017;8(1):286.

[70] Covarrubias AJ, Aksoylar HI, Horng T. Control of macrophage metabolism and activation by mTOR and Akt signaling. Semin Immunol 2015;27(4):286–96.

[71] Eshghjoo S, Kim DM, Jayaraman A, Sun Y, Alaniz RC. Macrophage polarization in atherosclerosis. Genes 2022;13(5).

[72] Kracht M, Muller-Ladner U, Schmitz ML. Mutual regulation of metabolic processes and proinflammatory NF-kappaB signaling. J Allergy Clin Immunol 2020;146(4):694–705.

[73] Capece D, Verzella D, Flati I, Arboretto P, Cornice J, Franzoso G. NF-kappaB: blending metabolism, immunity, and inflammation. Trends Immunol 2022;43(9):757–75.

[74] Xu J, Gao C, He Y, Fang X, Sun D, Peng Z, et al. NLRC3 expression in macrophage impairs glycolysis and host immune defense by modulating the NF-kappaB-NFAT5 complex during septic immunosuppression. Mol Ther 2023;31(1):154–73.

[75] Mauer J, Chaurasia B, Plum L, Quast T, Hampel B, Blüher M, et al. Myeloid cell-restricted insulin receptor deficiency protects against obesity-induced inflammation and systemic insulin resistance. PLoS Genet 2010;6(5): e1000938.

[76] Arranz A, Doxaki C, Vergadi E, Martinez de la Torre Y, Vaporidi K, Lagoudaki ED, et al. Akt1 and Akt2 protein kinases differentially contribute to macrophage polarization. Proc Natl Acad Sci U S A 2012;109(24):9517–22.

[77] Law NC, White MF, Hunzicker-Dunn ME. G protein-coupled receptors (GPCRs) that signal via protein kinase A (PKA) cross-talk at insulin receptor substrate 1 (IRS1) to activate the phosphatidylinositol 3-kinase (PI3K)/AKT pathway. J Biol Chem 2016;291(53):27160–9.

[78] Hunzicker-Dunn ME, Lopez-Biladeau B, Law NC, Fiedler SE, Carr DW, Maizels ET. PKA and GAB2 play central roles in the FSH signaling pathway to PI3K and AKT in ovarian granulosa cells. Proc Natl Acad Sci U S A 2012;109(44):E2979–88.

[79] Dalle S, Quoyer J, Varin E, Costes S. Roles and regulation of the transcription factor CREB in pancreatic β-cells. Curr Mol Pharmacol 2011;4(3):187–95.

[80] Jhala US, Canettieri G, Screaton RA, Kulkarni RN, Krajewski S, Reed J, et al. cAMP promotes pancreatic beta-cell survival via CREB-mediated induction of IRS2. Genes Dev 2003;17(13):1575–80.

[81] Luo N, Liu J, Chung BH, Yang Q, Klein RL, Garvey WT, et al. Macrophage adiponectin expression improves insulin sensitivity and protects against inflammation and atherosclerosis. Diabetes 2010;59(4):791–9.

[82] Law IK, Xu A, Lam KS, Berger T, Mak TW, Vanhoutte PM, et al. Lipocalin-2 deficiency attenuates insulin resistance associated with aging and obesity. Diabetes 2010;59(4):872–82.

[83] Sun Y, Butte NF, Garcia JM, Smith RG. Characterization of adult ghrelin and ghrelin receptor knockout mice under positive and negative energy balance. Endocrinology 2008;149(2):843–50.

[84] Li H, Wu G, Fang Q, Zhang M, Hui X, Sheng B, et al. Fibroblast growth factor 21 increases insulin sensitivity through specific expansion of subcutaneous fat. Nat Commun 2018;9(1):1–16.

[85] Rui L. Energy metabolism in the liver. Compr Physiol 2014;4(1):177–97.

[86] Liu Y, Lu X, Li X, Du P, Qin G. High-fat diet triggers obesity-related early infiltration of macrophages into adipose tissue and transient reduction of blood monocyte count. Mol Immunol 2020;117:139–46.

[87] Morinaga H, Mayoral R, Heinrichsdorff J, Osborn O, Franck N, Hah N, et al. Characterization of distinct subpopulations of hepatic macrophages in HFD/obese mice. Diabetes 2014;64(4):1120–30.

[88] Yang CY, Chen JB, Tsai TF, Tsai YC, Tsai CY, Liang PH, et al. CLEC4F is an inducible C-type lectin in F4/80-positive cells and is involved in alpha-galactosylceramide presentation in liver. PLoS One 2013;8(6):e65070.

[89] Remmerie A, Martens L, Thoné T, Castoldi A, Seurinck R, Pavie B, et al. Osteopontin expression identifies a subset of recruited macrophages distinct from Kupffer cells in the fatty liver. Immunity 2020;53(3):641–657.e614.

[90] Lam D, Harris D, Qin Z. Inflammatory mediator profiling reveals immune properties of chemotactic gradients and macrophage mediator production inhibition during thioglycollate elicited peritoneal inflammation. Mediat Inflamm 2013;2013.

[91] Elgazar-Carmon V, Rudich A, Hadad N, Levy R. Neutrophils transiently infiltrate intra-abdominal fat early in the course of high-fat feeding. J Lipid Res 2008;49(9):1894–903.

[92] Lee YS, Li P, Huh JY, Hwang IJ, Lu M, Kim JI, et al. Inflammation is necessary for long-term but not short-term high-fat diet–induced insulin resistance. Diabetes 2011;60(10):2474–83.

[93] Patsouris D, Li PP, Thapar D, Chapman J, Olefsky JM, Neels JG. Ablation of CD11c-positive cells normalizes insulin sensitivity in obese insulin resistant animals. Cell Metab 2008;8(4):301–9.

[94] Han MS, Jung DY, Morel C, Lakhani SA, Kim JK, Flavell RA, et al. JNK expression by macrophages promotes obesity-induced insulin resistance and inflammation. Science 2013;339(6116):218–22.

[95] O'Neill LA, Kishton RJ, Rathmell J. A guide to immunometabolism for immunologists. Nat Rev Immunol 2016;16(9):553.

[96] Prieur X, Mok CY, Velagapudi VR, Nunez V, Fuentes L, Montaner D, et al. Differential lipid partitioning between adipocytes and tissue macrophages modulates macrophage lipotoxicity and M2/M1 polarization in obese mice. Diabetes 2011;60(3):797–809.

[97] Finucane OM, Sugrue J, Rubio-Araiz A, Guillot-Sestier M-V, Lynch MA. The NLRP3 inflammasome modulates glycolysis by increasing PFKFB3 in an IL-1β-dependent manner in macrophages. Sci Rep 2019;9(1):4034.

[98] Luan B, Yoon YS, Le Lay J, Kaestner KH, Hedrick S, Montminy M. CREB pathway links PGE2 signaling with macrophage polarization. Proc Natl Acad Sci U S A 2015;112(51):15642–7.

[99] Negreiros-Lima GL, Lima KM, Moreira IZ, Jardim BLO, Vago JP, Galvão I, et al. Cyclic AMP regulates key features of macrophages via PKA: recruitment, reprogramming and efferocytosis. Cells 2020;9(1).

[100] Baumgartl J, Baudler S, Scherner M, Babaev V, Makowski L, Suttles J, et al. Myeloid lineage cell-restricted insulin resistance protects apolipoproteinE-deficient mice against atherosclerosis. Cell Metab 2006;3(4):247–56.

[101] Knuever J, Willenborg S, Ding X, Akyuz MD, Partridge L, Niessen CM, et al. Myeloid cell-restricted insulin/IGF-1 receptor deficiency protects against skin inflammation. J Immunol 2015;195(11):5296—308.

[102] Ji Y, Dai Z, Sun S, Ma X, Yang Y, Tso P, et al. Hydroxyproline attenuates dextran sulfate sodium-induced colitis in mice: involvment of the NF-kappaB signaling and oxidative stress. Mol Nutr Food Res 2018;62(21): e1800494.

[103] Okamoto M, Suzuki T, Mizukami Y, Ikeda T. The membrane-type estrogen receptor G-protein-coupled estrogen receptor suppresses lipopolysaccharide-induced interleukin 6 via inhibition of nuclear factor-kappa B pathway in murine macrophage cells. Anim Sci J 2017;88(11):1870—9.

[104] Cuellar JN, Isokawa M. Ghrelin-induced activation of cAMP signal transduction and its negative regulation by endocannabinoids in the hippocampus. Neuropharmacology 2011;60(6):842—51.

[105] Huang C, Thirone AC, Huang X, Klip A. Differential contribution of insulin receptor substrates 1 versus 2 to insulin signaling and glucose uptake in l6 myotubes. J Biol Chem 2005;280(19):19426—35.

[106] Abdelli S, Bonny C. JNK3 maintains expression of the insulin receptor substrate 2 (IRS2) in insulin-secreting cells: functional consequences for insulin signaling. PLoS One 2012;7(5):e35997.

[107] Vergadi E, Ieronymaki E, Lyroni K, Vaporidi K, Tsatsanis C. Akt signaling pathway in macrophage activation and M1/M2 polarization. J Immunol 2017;198(3):1006—14.

[108] Babaev VR, Hebron KE, Wiese CB, Toth CL, Ding L, Zhang Y, et al. Macrophage deficiency of Akt2 reduces atherosclerosis in Ldlr null mice. J Lipid Res 2014;55(11):2296—308.

[109] Hendrikx T, Porsch F, Kiss MG, Rajcic D, Papac-Milićević N, Hoebinger C, et al. Soluble TREM2 levels reflect the recruitment and expansion of TREM2+ macrophages that localize to fibrotic areas and limit NASH. J Hepatol 2022;77(5):1373—85.

[110] Briggs DI, Enriori PJ, Lemus MB, Cowley MA, Andrews ZB. Diet-induced obesity causes ghrelin resistance in arcuate NPY/AgRP neurons. Endocrinology 2010;151(10):4745—55.

[111] English PJ, Ghatei MA, Malik IA, Bloom SR, Wilding JP. Food fails to suppress ghrelin levels in obese humans. J Clin Endocrinol Metab 2002;87(6):2984.

[112] Naznin F, Toshinai K, Waise TM, NamKoong C, Md Moin AS, Sakoda H, et al. Diet-induced obesity causes peripheral and central ghrelin resistance by promoting inflammation. J Endocrinol 2015;226(1):81—92.

[113] Beiras-Fernandez A, Kreth S, Weis F, Ledderose C, Pöttinger T, Dieguez C, et al. Altered myocardial expression of ghrelin and its receptor (GHSR-1a) in patients with severe heart failure. Peptides 2010;31(12):2222—8.

[114] Wu R, Zhou M, Cui X, Simms HH, Wang P. Upregulation of cardiovascular ghrelin receptor occurs in the hyperdynamic phase of sepsis. Am J Physiol Heart Circ Physiol 2004;287(3):H1296—302.

[115] Demers A, Caron V, Rodrigue-Way A, Wahli W, Ong H, Tremblay A. A concerted kinase interplay identifies PPARgamma as a molecular target of ghrelin signaling in macrophages. PLoS One 2009;4(11):e7728.

[116] Li WG, Gavrila D, Liu X, Wang L, Gunnlaugsson S, Stoll LL, et al. Ghrelin inhibits proinflammatory responses and nuclear factor-kappaB activation in human endothelial cells. Circulation 2004;109(18):2221—6.

[117] Zhao D, Zhan Y, Zeng H, Moyer MP, Mantzoros CS, Pothoulakis C. Ghrelin stimulates interleukin-8 gene expression through protein kinase C-mediated NF-kappaB pathway in human colonic epithelial cells. J Cell Biochem 2006;97(6):1317—27.

[118] Siegl D, Midura EF, Annecke T, Conzen P, Caldwell CC, Tschoep J. The effect of ghrelin upon the early immune response in lean and obese mice during sepsis. PLoS One 2015;10(4):e0122211.

[119] Waseem T, Duxbury M, Ito H, Ashley SW, Robinson MK. Exogenous ghrelin modulates release of pro-inflammatory and anti-inflammatory cytokines in LPS-stimulated macrophages through distinct signaling pathways. Surgery 2008;143(3):334—42.

[120] Au CC, Docanto MM, Zahid H, Raffaelli F-M, Ferrero RL, Furness JB, et al. Des-acyl ghrelin inhibits the capacity of macrophages to stimulate the expression of aromatase in breast adipose stromal cells. J Steroid Biochem Mol Biol 2017;170:49—53.

[121] Yuan F, Ma J, Xiang X, Lan H, Xu Y, Zhao J, et al. Improvement of adipose macrophage polarization in high fat diet-induced obese GHSR knockout mice. BioMed Res Int 2018;2018:4924325.

[122] Davies JS, Kotokorpi P, Eccles SR, Barnes SK, Tokarczuk PF, Allen SK, et al. Ghrelin induces abdominal obesity via GHS-R-dependent lipid retention. Mol Endocrinol 2009;23(6):914—24.

[123] Ma X, Lin L, Qin G, Lu X, Fiorotto M, Dixit VD, et al. Ablations of ghrelin and ghrelin receptor exhibit differential metabolic phenotypes and thermogenic capacity during aging. PLoS One 2011;6(1):e16391.

[124] Delhanty PJ, van der Eerden BC, van der Velde M, Gauna C, Pols HA, Jahr H, et al. Ghrelin and unacylated ghrelin stimulate human osteoblast growth via mitogen-activated protein kinase (MAPK)/phosphoinositide 3-kinase (PI3K) pathways in the absence of GHS-R1a. J Endocrinol 2006;188(1):37—47.

[125] Gauna C, Delhanty PJ, Hofland LJ, Janssen JA, Broglio F, Ross RJ, et al. Ghrelin stimulates, whereas des-octanoyl ghrelin inhibits, glucose output by primary hepatocytes. J Clin Endocrinol Metab 2005;90(2):1055—60.

[126] Damian M, Marie J, Leyris JP, Fehrentz JA, Verdie P, Martinez J, et al. High constitutive activity is an intrinsic feature of ghrelin receptor protein: a study with a functional monomeric GHS-R1a receptor reconstituted in lipid discs. J Biol Chem 2012;287(6):3630—41.

[127] Ma X, Lin L, Yue J, Wu CS, Guo CA, Wang R, et al. Suppression of ghrelin exacerbates HFCS-induced adiposity and insulin resistance. Int J Mol Sci 2017;18(6).

[128] Mear Y, Enjalbert A, Thirion S. GHS-R1a constitutive activity and its physiological relevance. Front Neurosci 2013;7:87.

[129] Kern A, Mavrikaki M, Ullrich C, Albarran-Zeckler R, Brantley AF, Smith RG. Hippocampal dopamine/DRD1 signaling dependent on the ghrelin receptor. Cell 2015;163(5):1176—90.